

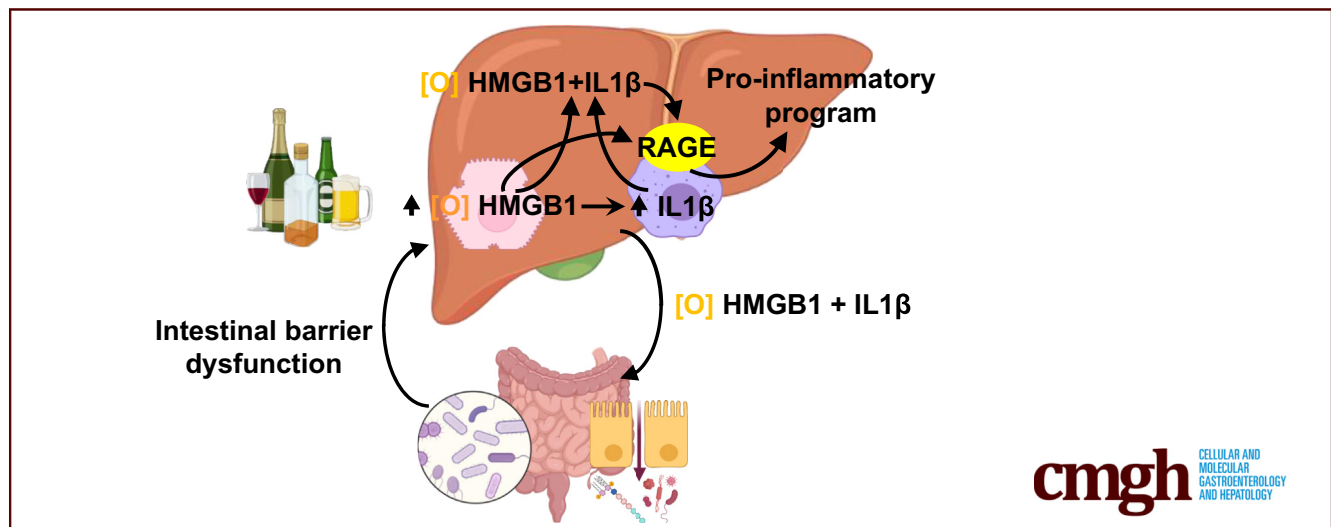
## ORIGINAL RESEARCH

## A Protein Complex of Liver Origin Activates a Pro-inflammatory Program That Drives Hepatic and Intestinal Injury in Alcohol-Associated Liver Disease



Xiaodong Ge,<sup>1</sup> Hui Han,<sup>1</sup> Romain Desert,<sup>1</sup> Sukanta Das,<sup>1</sup> Zhuolun Song,<sup>1</sup> Sai Santosh Babu Komakula,<sup>1</sup> Wei Chen,<sup>1</sup> Dipti Athavale,<sup>1</sup> Daniel Lantvit,<sup>1</sup> and Natalia Nieto<sup>1,2,3</sup>

<sup>1</sup>Department of Pathology, University of Illinois Chicago, Chicago, Illinois; <sup>2</sup>Department of Medicine, Division of Gastroenterology and Hepatology, University of Illinois Chicago, Chicago, Illinois; and <sup>3</sup>Research & Development Service, Jesse Brown Veterans Affairs Medical Center, Chicago, Illinois



## SUMMARY

In this study, we identified a mechanism whereby the liver-to-gut axis contributes to alcohol-associated liver disease. We found that the protein complex of hepatocyte-derived [O] HMGB1 with IL-1 $\beta$  activates a pro-inflammatory program that, besides being detrimental to the liver, drives intestinal barrier dysfunction; therefore, targeting this complex could have significant therapeutic potential.

**BACKGROUND & AIMS:** There is limited information on how the liver-to-gut axis contributes to alcohol-associated liver disease (AALD). We previously identified that high-mobility group box-1 (HMGB1) undergoes oxidation in hepatocytes and demonstrated elevated serum levels of oxidized HMGB1 ([O] HMGB1) in alcoholic patients. Since interleukin-1 beta (IL-1 $\beta$ ) increases in AALD, we hypothesized hepatocyte-derived [O] HMGB1 could interact with IL-1 $\beta$  to activate a pro-inflammatory program that, besides being detrimental to the liver, drives intestinal barrier dysfunction.

**RESULTS:** Alcohol-fed *Rage*<sup>ΔMye</sup> mice exhibited decreased nuclear factor kappa B signaling, a pro-inflammatory

signature, and reduced total intestinal permeability, resulting in protection from AALD. In addition, [O] HMGB1 bound and signaled through the receptor for advanced-glycation end-products (RAGE) in myeloid cells, driving hepatic inflammation, intestinal permeability, and increased portal blood lipopolysaccharide in AALD. We identified that [O] HMGB1 formed a complex with IL-1 $\beta$ , which was found in the livers of patients with acute alcoholic hepatitis and mice with AALD. This complex originated from the liver, because it was absent in the intestine when hepatocytes did not produce [O] HMGB1. Mechanistically, the complex bound RAGE in Kupffer cells and macrophages induced a pro-inflammatory program. Moreover, it bound RAGE in intestinal macrophages and epithelial cells, leading to intestinal inflammation, altered intestinal epithelial cell tight junction protein expression, increased intestinal permeability, and elevated portal blood lipopolysaccharide, enhancing AALD pathogenesis.

**CONCLUSIONS:** We identified a protein complex of liver origin that amplifies the pro-inflammatory feedback loop in AALD; therefore, targeting this complex could have significant therapeutic potential. (*Cell Mol Gastroenterol Hepatol* 2024;18:101362; <https://doi.org/10.1016/j.jcmgh.2024.05.010>)

**Keywords:** Disulfide High-Mobility Group Box-1; Interleukin-1 Beta; Intestinal Epithelial Cells; Macrophages; Receptor for Advanced-Glycation End-Products.

Alcohol-associated liver disease (AALD) represents a significant clinical problem and stands as a major cause of morbidity and mortality worldwide. The most effective therapy is alcohol abstinence. However, current treatment options for patients with severe acute alcoholic hepatitis (AAH) and patients struggling to achieve abstinence remain suboptimal.<sup>1</sup> Inflammation emerges as a hallmark of alcohol-induced liver injury.<sup>2–4</sup> The presence of inflammatory cells in early biopsies from alcoholic patients predicts disease progression.<sup>4</sup> Among patients with AALD, there is a notable activation of Kupffer cells (KCs) and infiltrated macrophages (MFs), coupled with increased production of disulfide high-mobility group box-1 ([O] HMGB1)<sup>5</sup> and interleukin-1 beta (IL-1B).<sup>6,7</sup> Chronic alcohol consumption exacerbates intestinal permeability and promotes lipopolysaccharide (LPS) translocation, further activating KCs and MFs to enhance the production of pro-inflammatory cytokines. The close link between the pro-inflammatory effects of alcohol and injury strongly supports efforts to target the immune reaction early for hepatic protection<sup>8</sup>; however, efficient upstream anti-inflammatory therapies are urgently needed.

Numerous studies have established the role of the gut-to-liver axis.<sup>9–15</sup> Still, there needs to be more information on how the liver-to-gut axis contributes to inflammation and injury in AALD. It remains unknown whether ethanol-induced sterile damage-associated molecular patterns (DAMPs) of liver origin activate a pro-inflammatory program that, besides being detrimental to the liver, drives intestinal barrier dysfunction, creating an amplifying pro-inflammatory feedback loop in AALD.

HMGB1 gained significant attention in the immunity field after its discovery as a potent endogenous initiator of inflammation.<sup>5,16–18</sup> HMGB1 is an emerging prototype DAMP<sup>19–21</sup> because it mediates systemic inflammation, is chemotactic,<sup>22</sup> triggers classic inflammatory responses in immune cells, and transduces signals to the host of cellular damage or immune cell activation via interaction with several cell surface receptors, including the receptor for advanced-glycation end-products (RAGE)<sup>23–25</sup> and toll-like receptor-4 (TLR4).<sup>26</sup> Yet, post-translational modifications of HMGB1 govern receptor binding and downstream signaling events.<sup>5,24,27–30</sup>

We previously demonstrated that HMGB1 is up-regulated in response to liver injury and participates in the pathogenesis of AALD.<sup>5</sup> Moreover, we identified that native HMGB1 ([H] HMGB1) undergoes oxidation in hepatocytes (HEPs) and found that serum levels of [O] HMGB1 increase in alcoholic patients.<sup>5</sup> In addition, IL-1B is highly elevated in AALD.<sup>6,7,31,32</sup> Although attempts were made to block IL-1R to prevent AALD,<sup>7</sup> success was limited because of increasing the availability of circulating IL-1B, among others. To date, it is unknown whether HEP-derived [O] HMGB1 interacts with IL-1B to enhance the pathogenesis of AALD.


We posited that HEP-derived [O] HMGB1 could interact with IL-1B. Indeed, we identified that [O] HMGB1 formed a complex with IL-1B. We found that this complex is of liver origin and binds RAGE in KCs and MFs to induce a pro-inflammatory program that exacerbates hepatic injury. By binding RAGE in intestinal MFs and epithelial cells (IECs) and/or inducing the pro-inflammatory program, this complex alters IEC tight junction (TJ) protein expression and increases intestinal barrier dysfunction. Our overarching goal was to dissect the pathogenic role of this complex of liver origin in regulating a pro-inflammatory program that drives hepatic and intestinal injury in AALD.

## Results

### *Alcohol-fed $Rage^{\Delta Mye}$ Mice Show a Decrease in Nuclear Factor Kappa B Signaling, a Pro-Inflammatory Signature, and Total Intestinal Permeability, Which Results in Protection From AALD*

Among the receptors HMGB1 binds to, RAGE and TLR4 participate in liver disease<sup>33,34</sup>; therefore, we analyzed them by quantitative polymerase chain reaction (qPCR) and found similar expression in livers of wild-type (WT) mice fed control or ethanol Lieber-DeCarli (LDC) diet (not shown). To determine whether RAGE and TLR4 signaling in myeloid cells (Mye) participate in AALD, WT, conditional *Rage* knockout mice in myeloid cells (*Rage* <sup>$\Delta Mye$</sup> ), and conditional *Tlr4* knockout mice in myeloid cells (*Tlr4* <sup>$\Delta Mye$</sup> ) mice were fed a control or ethanol LDC diet for 6 weeks. Liver injury was prevented in ethanol-fed *Rage* <sup>$\Delta Mye$</sup>  compared with WT and *Tlr4* <sup>$\Delta Mye$</sup>  mice, as shown by H&E staining (Figure 1A, top), histopathologic scores (steatosis, hepatocyte ballooning degeneration, inflammation), and parameters of liver injury (liver-to-body weight ratios, serum alanine aminotransferase [ALT] activities, liver triglycerides) (Figure 1B). HMGB1 expression increased similarly in all ethanol-fed mice (Figure 1A bottom and 1B middle).

**Abbreviations used in this paper:** [H] HMGB1, native or fully reduced HMGB1; [O] HMGB1, disulfide or oxidized HMGB1; AAH, acute alcoholic hepatitis; AALD, alcohol-associated liver disease; AAV8, adeno-associated virus serotype-8; Ab, antibody; Alb, albumin; ALT, alanine aminotransferase; BSA, bovine serum albumin; DAMP, damage-associated molecular pattern; ELISA, enzyme-linked immunosorbent assay; HEPs, hepatocytes; HMGB1, high-mobility group box-1; *Hmgb1*<sup>*fl/fl*</sup>, *Hmgb1* floxed mice; IEC, intestinal epithelial cell; IHC, immunohistochemistry; IL-1B, interleukin-1 beta; IPA, Ingenuity Pathway Analysis; KC, Kupffer cell; LDC, Lieber-DeCarli diet; LPS, lipopolysaccharide; MF, macrophage; Mye, myeloid cell; NF- $\kappa$ B, nuclear factor kappa B; PLA, proximity ligation assay; qPCR, quantitative real-time polymerase chain reaction; RAGE, receptor for advanced-glycation end-products; *Rage*<sup>*fl/fl*</sup>, *Rage* floxed mice; RNA-seq, RNA sequencing; SEM, standard error of the mean; *Tbg*, thyroxine-binding globulin; TJ, tight junction; TLR4, toll-like receptor-4; *Tlr4* <sup>$\Delta Mye$</sup> , conditional *Tlr4* knockout mice in myeloid cells; TNFA, tumor necrosis factor- $\alpha$ ; WT, wild-type;  $\Delta$ [O] HMGB1, oxidation-incompetent HMGB1 mutant.

 Most current article

© 2024 The Authors. Published by Elsevier Inc. on behalf of the AGA Institute. This is an open access article under the CC BY-NC-ND license (<http://creativecommons.org/licenses/by-nc-nd/4.0/>).

2352-345X

<https://doi.org/10.1016/j.jcmgh.2024.05.010>

To understand the mechanism by which *Rage* ablation in Mye protects from AALD, we performed liver RNA sequencing (RNA-seq), revealing the induction of nuclear factor kappa B (NF $\kappa$ B) signaling and pro-inflammatory genes (CCL2/3/5, CX3CL1) in livers from ethanol-fed WT but not *Rage*<sup>ΔMye</sup> mice (Figure 1C). Changes in the pro-inflammatory genes were also confirmed at the protein level (Figure 1D). Next, we evaluated intestinal events that could contribute to AALD. The increase in intestinal injury, total intestinal permeability, portal blood LPS, and pathologic score was prevented in ethanol-fed *Rage*<sup>ΔMye</sup> compared with WT mice (Figure 1E and F and Figure 2A and B). These results suggest that RAGE signaling in Mye is essential for hepatic inflammation and increased intestinal permeability in AALD.

### [O] HMGB1 Binds RAGE

We previously found elevated [O] HMGB1 in alcoholic patients and mice with AALD.<sup>5</sup> However, whether [O] HMGB1 is a ligand for RAGE, either alone or in complex with other proteins increased in AALD and the signals it conveys in Mye (ie, KCs and MFs) to induce the pro-inflammatory program and in IECs to increase intestinal permeability, remain to be determined. First, we used surface plasmon resonance to test whether [O] HMGB1 binds RAGE. RAGE was captured on a CM5 sensor chip surface, and [O] HMGB1 was added at increasing concentrations from 0–8 μmol/L for 5 minutes to generate sensorgrams. The association rate constant  $k_a = 5.10 (\pm 1.70) \times 10^3 \text{ mol/L}^{-1}\text{s}^{-1}$ , dissociation rate constant  $k_d = 1.22 (\pm 0.49) \times 10^{-2} \text{ s}^{-1}$ , and equilibrium dissociation constant  $K_D = 2.39 \pm 0.43 \text{ μmol/L}$  were calculated by fitting the data to the 1:1 Langmuir kinetic binding model. The  $K_D = 2.6 \pm 0.7 \text{ μmol/L}$  was also calculated by steady-state affinity. Response at equilibrium was plotted against time and concentration (Figure 3A). These results suggest that [O] HMGB1 has a significant affinity for RAGE, and that the binding is stable over time and dose-dependent.

### [O] HMGB1 Signals via RAGE in Myeloid Cells to Drive Hepatic Inflammation, Intestinal Permeability, and Increased Portal Blood LPS in AALD

We used two approaches to prove that [O] HMGB1 binding to RAGE in Mye occurs in vivo. First, we injected WT and *Rage*<sup>ΔMye</sup> mice with bovine serum albumin (BSA) (control), [H] HMGB1, or [O] HMGB1 while feeding them the ethanol LDC diet for 6 weeks. WT mice injected [O] HMGB1 displayed increased liver injury (as shown by H&E staining, histopathologic scores, and parameters of liver injury) (Figure 3B and C), the pro-inflammatory signature in liver (Figure 3D), intestinal injury (Figure 3E), and parameters of intestinal injury (total intestinal permeability, portal blood LPS, pathologic scores) (Figure 3F), compared with WT mice injected BSA or [H] HMGB1, or with *Rage*<sup>ΔMye</sup> mice injected [O] HMGB1. HMGB1 expression increased equally in all mice (Figure 3B bottom and 3C middle).

Second, we transduced *Hmgb1&Rage*<sup>ΔHepΔMye</sup> mice with adeno-associated virus serotype-8 (AAV8) vectors containing a hepatocyte-specific promoter (thyroxine-binding

globulin, *Tbg*) to overexpress WT HMGB1 or Δ[O] HMGB1 in HEPs. *Hmgb1&Rage*<sup>ΔHepΔMye</sup> overexpressing WT HMGB1, which can undergo oxidation to produce [O] HMGB1, showed a similar pro-inflammatory signature in liver (Figure 4A), intestinal injury (Figure 4B), and parameters of intestinal injury (total intestinal permeability, portal blood LPS, pathologic scores) (Figure 4C), compared with mice overexpressing Δ[O] HMGB1, due to lack of RAGE in Mye. Thus, the data suggest that RAGE signaling in Mye contributes to the pro-inflammatory effects of [O] HMGB1 in AALD.

### [O] HMGB1 Forms a Complex With IL-1B, Found in the Livers and Serum of Patients With AAH and Mice With AALD

To assess whether the HMGB1 isoforms bind IL-1B, highly increased in AALD,<sup>6,7,31,32</sup> we incubated [H] HMGB1 or [O] HMGB1 with IL-1B alone to allow complexing or with neutralizing antibodies (Abs) to HMGB1 or IL-1B to prevent formation of the complex. Pull-down assays revealed that [O] HMGB1 strongly binds IL-1B, whereas [H] HMGB1 barely binds it. The interaction was blocked by either Ab, validating specificity (Figure 5A). This was further demonstrated by surface plasmon resonance. IL-1B was captured on a CM5 sensor chip surface, and [H] HMGB1 and [O] HMGB1 were injected at concentrations ranging from 0–8 μmol/L for 5 minutes to generate sensorgrams. For the interaction of [O] HMGB1 with IL-1B, the association rate constant  $k_a = 5.32 (\pm 0.26) \times 10^3 \text{ mol/L}^{-1}\text{s}^{-1}$ , the dissociation rate constant  $k_d = 1.87 (\pm 0.35) \times 10^{-2} \text{ s}^{-1}$ , and the equilibrium dissociation constant  $K_D = 3.53 \pm 0.87 \text{ μmol/L}$ , determined by fitting the data to the 1:1 Langmuir kinetic binding model and by steady-state affinity. For both interactions, responses at equilibrium were plotted against time and concentration. The data suggested that [O] HMGB1 strongly and dose-dependently binds IL-1B; however, [H] HMGB1 has a minimal binding affinity (Figure 5B). Binding was confirmed and enhanced in the livers and serum of patients with AAH and mice with AALD through immunoprecipitation for IL-1B and subsequent immunoblotting under non-reducing conditions to detect bound [O] HMGB1 (Figure 5C and D). Therefore, alcohol induces the formation of a complex between [O] HMGB1 and IL-1B, yet its pathogenic role in AALD remains unknown.

### The Complex Binds RAGE in the Liver and Jejunum From Ethanol-fed Mice

To determine the binding affinity of the complex for RAGE, we performed surface plasmon resonance. IL-1B was captured on a CM5 sensor chip surface, and [O] HMGB1 bound to RAGE was injected at ranging from 0–10 μmol/L for 5 minutes to generate sensorgrams. The  $k_a = 5.42 (\pm 1.15) \times 10^3 \text{ mol/L}^{-1}\text{s}^{-1}$ ,  $k_d = 3.69 (\pm 0.32) \times 10^{-3} \text{ s}^{-1}$ , and  $K_D = 0.70 \pm 0.10 \text{ μmol/L}$  constants were calculated by fitting the data to the 1:1 Langmuir kinetic binding model and steady-state affinity. Response at equilibrium was plotted against time and concentration. There was a binding affinity of the protein complex for RAGE (Figure 6A), although lower than by [O] HMGB1 alone (Figure 5B).

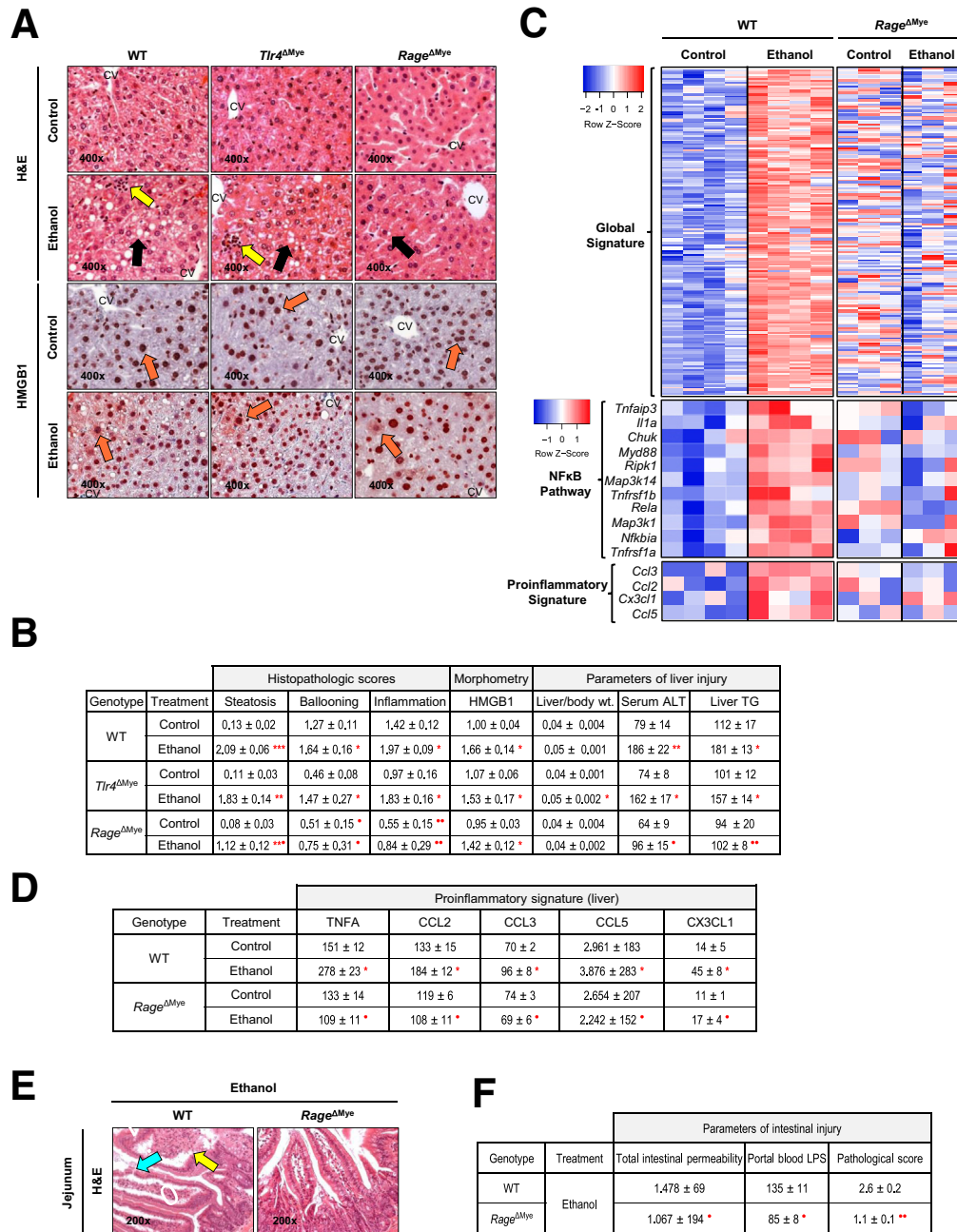


**Figure 1. Alcohol-fed *Rage*<sup>ΔMyc</sup> mice show a decrease in NFκB signaling, a pro-inflammatory signature, and total intestinal permeability, which results in protection from AALD.** WT (controls), *Rage*<sup>ΔMyc</sup>, and *Tlr4*<sup>ΔMyc</sup> mice were fed a control or an ethanol LDC diet for 6 weeks. H&E staining (black arrows: steatosis, yellow arrows: inflammation) (A top) and HMGB1 IHC (orange arrows: positive staining) (A bottom). Histopathologic scores (steatosis, hepatocyte ballooning degeneration, inflammation), HMGB1 morphometry, and parameters of liver injury (liver-to-body weight ratios, serum ALT activities, liver triglycerides) (B). Heatmaps from RNA-seq of the liver showing global, NFκB pathway, and pro-inflammatory gene signatures (red: up, blue: down) (C). Liver pro-inflammatory protein signature (TNFA, CCL2, and CCL5 are in pg/mg, CCL3 and CX3CL1 are in ng/mg) (D). Jejunum H&E staining (blue arrow: focal ulceration, yellow arrow: inflammation) (E). Parameters of intestinal injury (total intestinal permeability [FITC fluorescence units], portal blood LPS [pg/mL], pathologic scores) (F). Results are expressed as mean ± SEM; n = 6 male and n = 6 female/group. \**P* < .05, \*\**P* < .01, and \*\*\**P* < .001 vs Control; \**P* < .05 and \*\**P* < .01 vs WT.

Importantly, we also ruled out the binding of IL-1B to RAGE (Figure 7).

To investigate whether the complex binds RAGE in MFs, we performed proximity ligation assays (PLAs). This

approach confirmed that the complex binds RAGE in MFs isolated from the livers of WT mice but not from *Rage*<sup>ΔMyc</sup> mice (Figure 6B). Because we hypothesized that the liver signals to the intestine (ie, liver-to-gut axis), we investigated

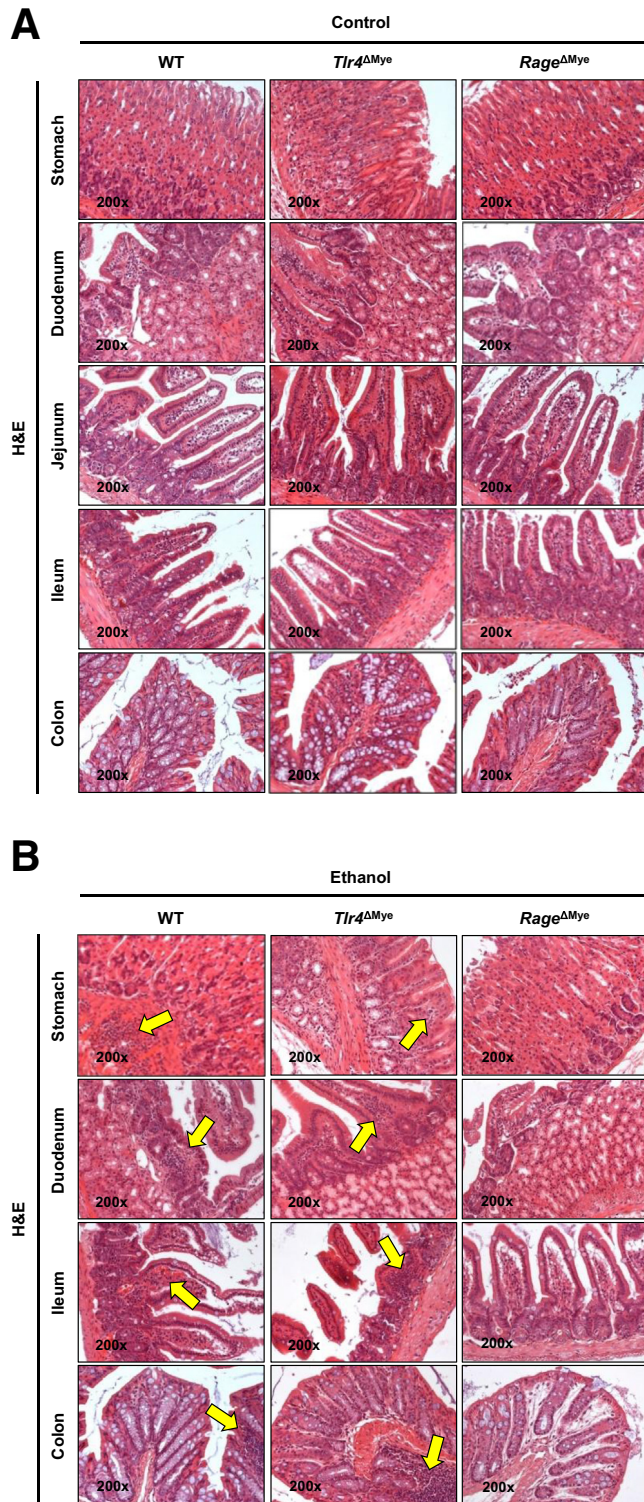


**Figure 2. Alcohol-fed  $Rage^{\Delta Myc}$  mice are protected from intestinal injury.** WT (controls),  $Rage^{\Delta Myc}$ , and  $Tlr4^{\Delta Myc}$  mice were fed a control or an ethanol LDC diet for 6 weeks. H&E staining of stomach, duodenum, jejunum, ileum, and colon in mice fed control (A) or ethanol (B) (yellow arrows: inflammation).  $n = 6$  male and  $n = 6$  female/group.

whether the complex is present in the intestine during AALD. To examine this, we performed PLAs on the intestine of WT and  $Hmgb1^{\Delta Hep\Delta Myc\Delta IEC}$  mice fed ethanol. The latter

mice were chosen to minimize the production of HMGB1 (negative control). We found that the complex is present in the intestine of ethanol-fed WT but not in mice unable to produce [O] HMGB1 (Figure 6C). Binding was specific because  $Hmgb1^{\Delta Hep\Delta Myc\Delta IEC}$  mice fed ethanol and injected with the complex showed positive staining in the PLA (Figure 6C, right panels). Finally, binding was further validated by pull-down assays in mouse liver and jejunum from control and ethanol-fed mice (Figure 6D). Thus, the complex binds RAGE in MFs, liver, and intestine, but its mechanism of signaling to enhance alcohol-induced liver and intestinal injury remains elusive.

### The Complex Stimulates the Production of the Pro-inflammatory Signature by KCs and MFs via RAGE

To investigate whether the complex enhances tumor necrosis factor-alpha (TNFA) production, significantly increased in AALD,<sup>35</sup> and demonstrates its pathogenic relevance, primary KCs were isolated from WT mice and treated with the complex or each component for 24 hours. The complex increased *Tnfa* mRNA and secreted TNFA protein more than its components (Figure 8A bar graphs and Western blot). Furthermore, primary KCs from WT mice produced more TNFA and CCL5 when stimulated by the complex compared with each component. This effect was attenuated by ablating *Rage* as validated by co-treatment with a RAGE-neutralizing Ab (not shown) (Figure 8A table). Similarly, MFs treated with the complex for 24 hours showed increased intracellular and secreted TNFA, comparable with LPS treatment, highlighting its pathophysiological relevance (Figure 8B). RNA-seq revealed that MFs treated with the complex for 24 hours increased the NF $\kappa$ B pathway and pro-inflammatory genes (Figure 8C), as in livers from ethanol-fed WT mice, which were attenuated in  $Rage^{\Delta Myc}$  mice (Figure 1C). Further analysis by Ingenuity Pathway Analysis (IPA) showed the up-regulation of pathways involved in cytokine storm, MF activation, and HMGB1 signaling (Figure 8D). To investigate whether RAGE drives the effects of the complex, we co-incubated MFs with each component of the complex alone or with the complex along with Abs against RAGE or IL-1B. Blocking RAGE but not IL-1B reduced the increase in intracellular and secreted TNFA and CCL3, along with secreted CCL2 and CCL5, mediated by the complex (Figure 8E). Higher doses of RAGE Ab may be required for full protection, but the data suggest the complex signals via RAGE in MFs. In summary, the effects of the complex are greater than those of its components, inducing a RAGE-dependent pro-inflammatory signature in KCs and MFs. However, it remains unknown whether the complex elicits a higher pro-inflammatory response via RAGE signaling in vivo and how it causes hepatic and intestinal injury.

### The Complex Is Absent in the Intestine When HEPs Do Not Produce [O] HMGB1

Next, we asked whether the complex, expected to originate from the liver, was present in the intestine. Pull-down

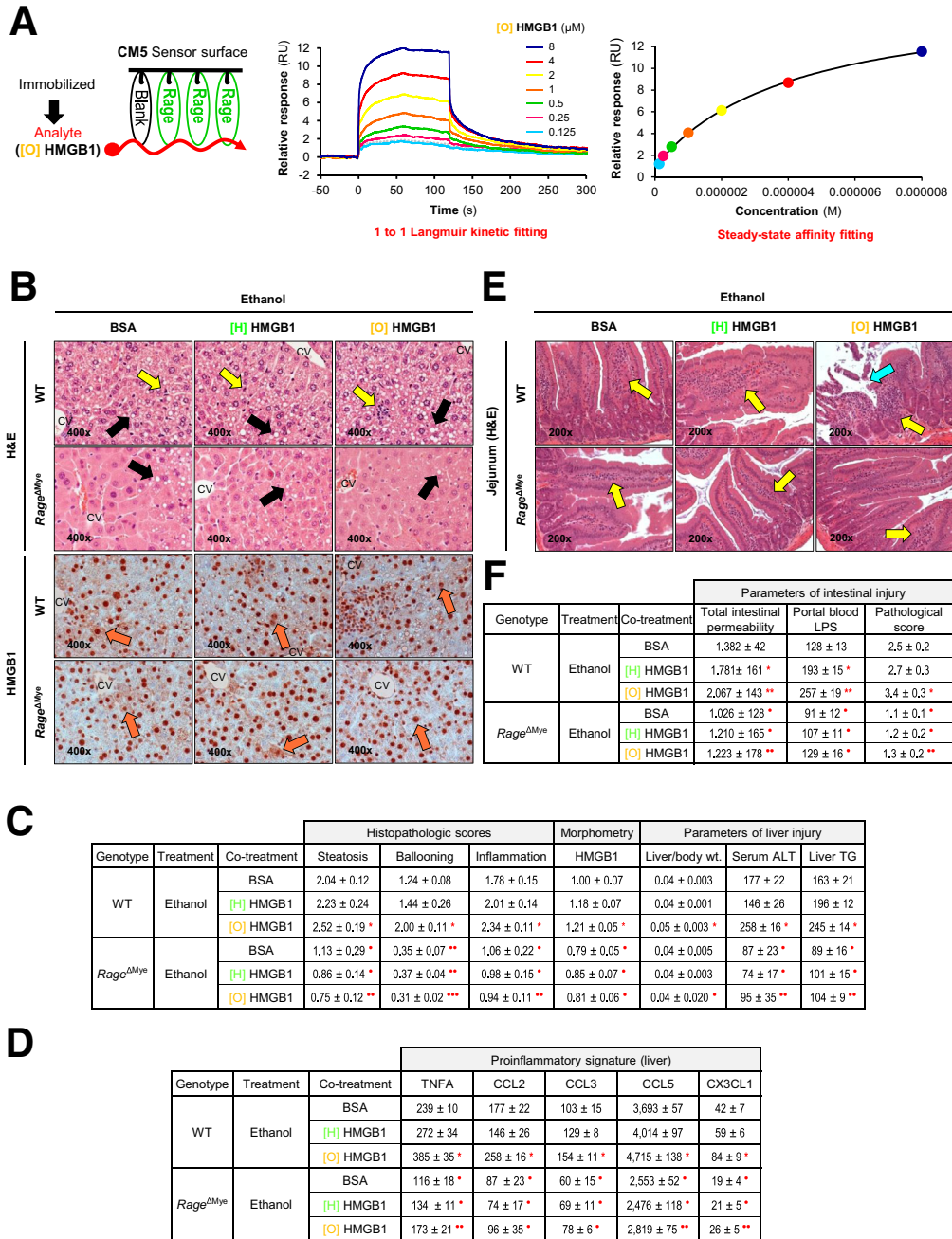


**Figure 3. [O] HMGB1 binds RAGE.** RAGE was captured on a CM5 sensor chip surface, and [O] HMGB1 was added at increasing concentrations from 0–8 μmol/L for 5 minutes (A left). Sensorgrams show the response at equilibrium plotted against time (A middle) and concentration (A right). [O] HMGB1 signals via RAGE in myeloid cells to drive hepatic inflammation, intestinal permeability, and increased portal blood LPS in AALD. WT (controls) and *Rage*<sup>ΔMye</sup> were injected with BSA (control), [H] HMGB1, or [O] HMGB1 and fed ethanol LDC diet for 6 weeks. H&E staining (black arrows: steatosis, yellow arrows: inflammation) (B top) and HMGB1 IHC (orange arrows: positive staining) (B bottom). Histopathologic scores (steatosis, hepatocyte ballooning degeneration, inflammation), HMGB1 morphometry, and parameters of liver injury (liver-to-body weight ratios, serum ALT activities, liver triglycerides) (C). Liver pro-inflammatory protein signature (TNFA, CCL2, and CCL5 are in pg/mg, CCL3 and CX3CL1 are in ng/mg) (D). Jejunum H&E staining (yellow arrows: inflammation, blue arrows: focal ulceration) (E). Parameters of intestinal injury (total intestinal permeability [FITC fluorescence units], portal blood LPS [pg/mL], pathologic scores) (F). In B–F, results are expressed as mean ± SEM; n = 6 male and n = 6 female/group. \*P < .05 and \*\*P < .01 vs BSA; \*P < .05, \*\*P < .01, and \*\*\*P < .001 vs WT.

assays demonstrated the presence of the complex in jejunum from ethanol-fed *Hmgb1*<sup>ΔHep</sup> mice, which express WT but not Δ[O] HMGB1 (Figure 9A left). In addition, we showed that

RAGE was unchanged in primary IECs treated with the complex (Figure 9A right). Thus, the complex is not found in the intestine when HEPs do not produce [O] HMGB1.

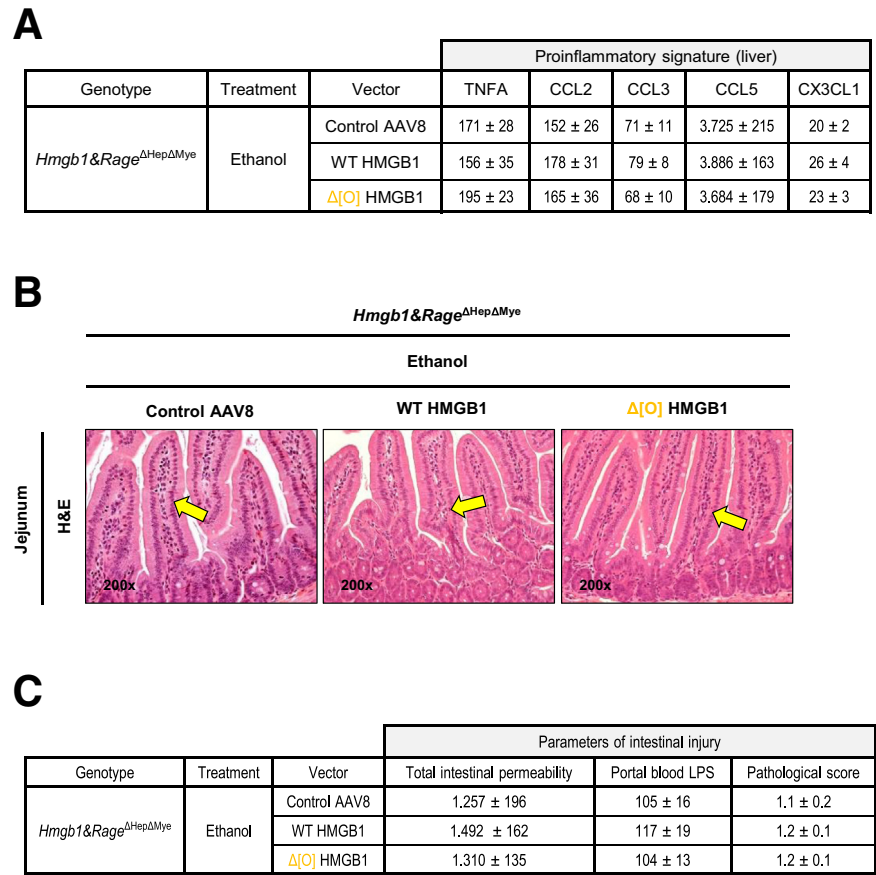


**Figure 4.** A second mouse model shows that [O] HMGB1 signals via RAGE in myeloid cells to drive AALD. *Hmgb1*&*Rage*<sup>ΔHepΔMye</sup> mice were transduced with AAV8 vectors to over-express WT HMGB1 or Δ[O] HMGB1 in HEPs or control vector. Two weeks later, mice were fed an ethanol LDC diet for 6 weeks. Liver pro-inflammatory protein signature (TNFA, CCL2, and CCL5 are in pg/mg; CCL3 and CX3CL1 are in ng/mg) (A). Jejunum H&E staining (yellow arrows: inflammation) (B). Parameters of intestinal injury (total intestinal permeability [FITC fluorescence units], portal blood LPS [pg/mL], pathologic scores) (C). Results are expressed as mean ± SEM; n = 6 male and n = 6 female/ group.

### The Complex Binds RAGE in Myeloid Cells and IECs to Increase Hepatic Inflammation and Intestinal Permeability and Enhance Portal Blood LPS in AALD

To assess whether the complex could signal via RAGE in myeloid cells and IECs to drive downstream effects, we injected it into WT (controls), *Rage*<sup>ΔMye</sup>, *Rage*<sup>ΔIEC</sup>, and *Rage*<sup>ΔIECΔMye</sup> mice throughout the ethanol-feeding regimen. *Rage*<sup>ΔIECΔMye</sup> mice exhibited significant protection from alcohol-induced liver injury compared with WT, *Rage*<sup>ΔMye</sup>, and *Rage*<sup>ΔIEC</sup> mice injected with the complex. Moreover, *Rage*<sup>ΔMye</sup> mice showed better protection than *Rage*<sup>ΔIEC</sup> mice. This was demonstrated by H&E staining (Figure 9B), histopathologic scores (steatosis, hepatocyte ballooning degeneration, inflammation), parameters of liver injury (liver-to-body weight ratios, serum ALT activity, liver triglycerides), and mortality rates (Figure 9C), and the pro-inflammatory signature in the liver (Figure 9D). Furthermore, *Rage*<sup>ΔIECΔMye</sup> mice displayed less alcohol-induced intestinal injury compared with WT, conditional *Rage* knockout mice in intestinal epithelial cells (*Rage*<sup>ΔIEC</sup>), conditional *Rage* knockout mice in intestinal epithelial cells and myeloid cells (*Rage*<sup>ΔIECΔMye</sup>), *Rage*<sup>ΔMye</sup>, and mice injected with the complex, as shown by H&E staining (Figures 10A and 11A), and decreased parameters of intestinal injury (total intestinal permeability, portal blood LPS, pathologic

scores) (Figure 10B). These results suggest that the complex signals via RAGE in Mye and IECs drive AALD pathogenesis.

### The Complex Alters IEC TJ Protein Expression

To determine whether the complex alters IEC TJ protein expression to increase intestinal permeability in vivo and whether this effect is receptor-dependent, we isolated IECs from WT (controls), *Rage*<sup>ΔMye</sup>, *Rage*<sup>ΔIEC</sup>, and *Rage*<sup>ΔIECΔMye</sup> mice injected with the complex. Western blot analysis showed induction of TJ proteins (CLDN7, ZO1, OCLN) in *Rage*<sup>ΔMye</sup>, *Rage*<sup>ΔIEC</sup>, and *Rage*<sup>ΔIECΔMye</sup> mice compared with WT mice. Injection of the complex reduced these TJ proteins more in *Rage*<sup>ΔIEC</sup> mice than in the other groups of mice (Figure 10C). This was validated by immunofluorescence in jejunal samples (Figure 10D), which also showed no effect on other TJ proteins (CLDN2, CLDN5) (Figure 11B). Therefore, the complex alters IEC TJ protein expression to increase intestinal permeability, which is prevented in *Rage*<sup>ΔMye</sup> and *Rage*<sup>ΔIECΔMye</sup> mice.

## Discussion

Previous work provides solid evidence that the gut-to-liver axis,<sup>9,10,36</sup> the composition of the gut microbiome,<sup>13,37,38</sup> and bile acids<sup>39,40</sup> are amenable targets to prevent AALD. However, a significant gap exists in the

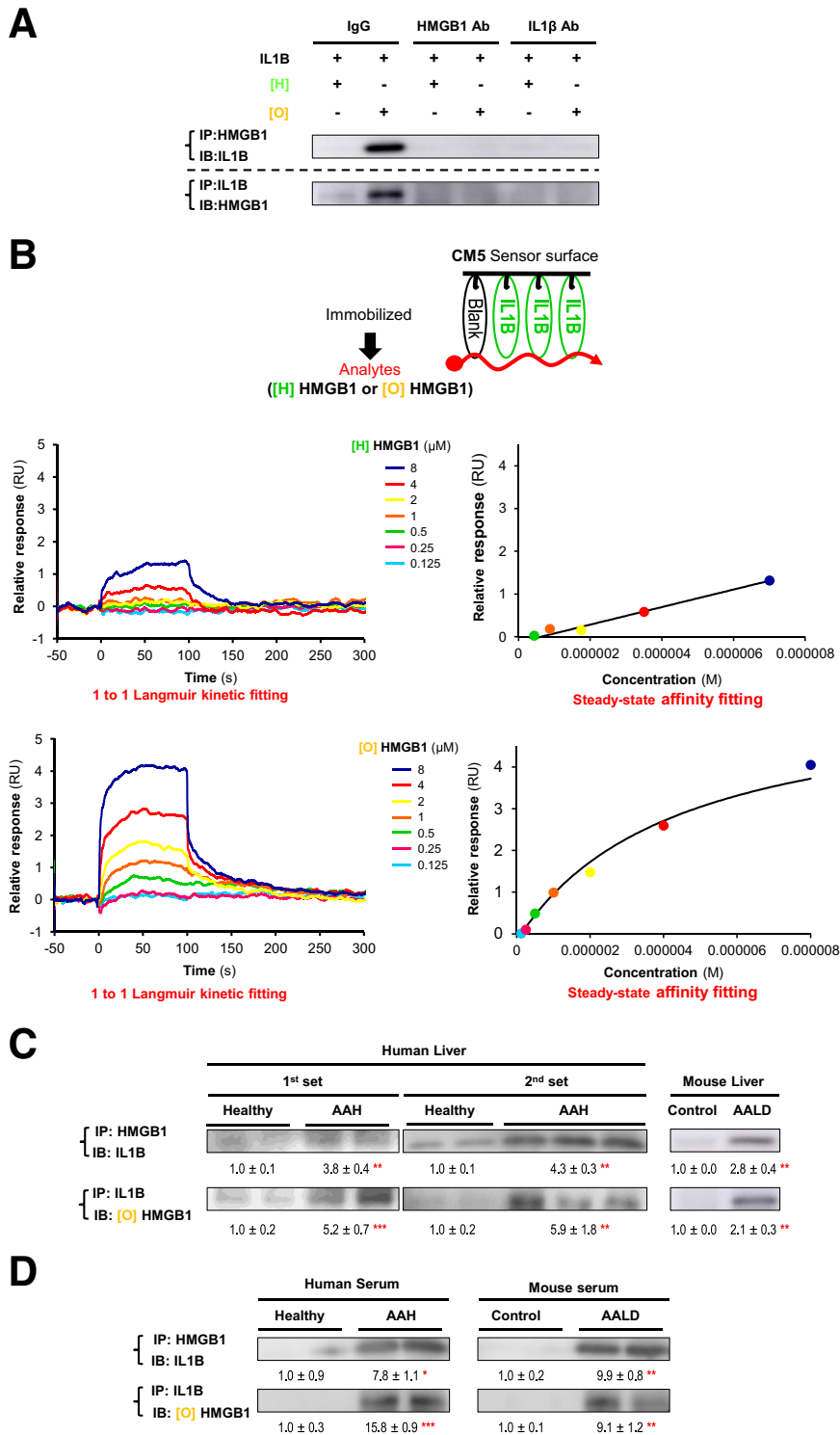


**Figure 5. [O] HMGB1 forms a complex with IL-1 $\beta$ , found in the livers and serum of patients with AAH and mice with AALD.** [H] HMGB1 and [O] HMGB1 were incubated with IL-1 $\beta$  (all at 1.5 nmol/L) and immunoglobulin G, HMGB1 Ab, or IL-1 $\beta$  Ab (all at 3  $\mu$ mol/L) for 1 hour at 37°C. Immunoprecipitation of HMGB1 and immunoblotting for IL-1 $\beta$  and the reverse (A). IL-1 $\beta$  was captured on a CM5 sensor chip surface, and [H] HMGB1 or [O] HMGB1 were injected at 0–8  $\mu$ mol/L for 5 minutes (B top). Sensorgrams show response at equilibrium plotted against time (B middle and bottom left) and concentration (B middle and bottom right). The amount of bound IL-1 $\beta$  and [O] HMGB1 in the livers of healthy and AAH patients was determined by immunoprecipitation of HMGB1 and immunoblotting for IL-1 $\beta$  and the reverse (C left). Bound [O] HMGB1 and IL1 $\beta$  in mice fed control or ethanol LDC diets for 6 weeks (C right). The amount of bound IL-1 $\beta$  and [O] HMGB1 in the serum of healthy and AAH patients was determined by immunoprecipitation of HMGB1 and immunoblotting for IL-1 $\beta$  and the reverse (D left). Bound [O] HMGB1 and IL-1 $\beta$  in serum of mice fed control or ethanol LDC diets for 6 weeks (D right). Results are expressed as mean  $\pm$  SEM; n = 6 Healthy and n = 6 AAH. n = 3 Control and n = 3 Ethanol. \* $P$  < .05, \*\* $P$  < .01, and \*\*\* $P$  < .001 vs Healthy or Control.

limited research addressing how the liver-to-gut axis,<sup>37</sup> specifically hepatic DAMPs, contributes to liver injury and intestinal permeability in AALD, which catalyzed this project.

Two key earlier findings from our laboratory laid the foundation for this study. Initially, we demonstrated that

HMGB1 is a DAMP up-regulated in response to liver injury, which participates in the pathogenesis of AALD.<sup>5</sup> Later, we found that HMGB1 undergoes oxidation in HEPs and that serum levels of [O] HMGB1 increase in alcoholic patients.<sup>5</sup> Therefore, how does the current study advance our knowledge of the role of [O] HMGB1 in AALD?



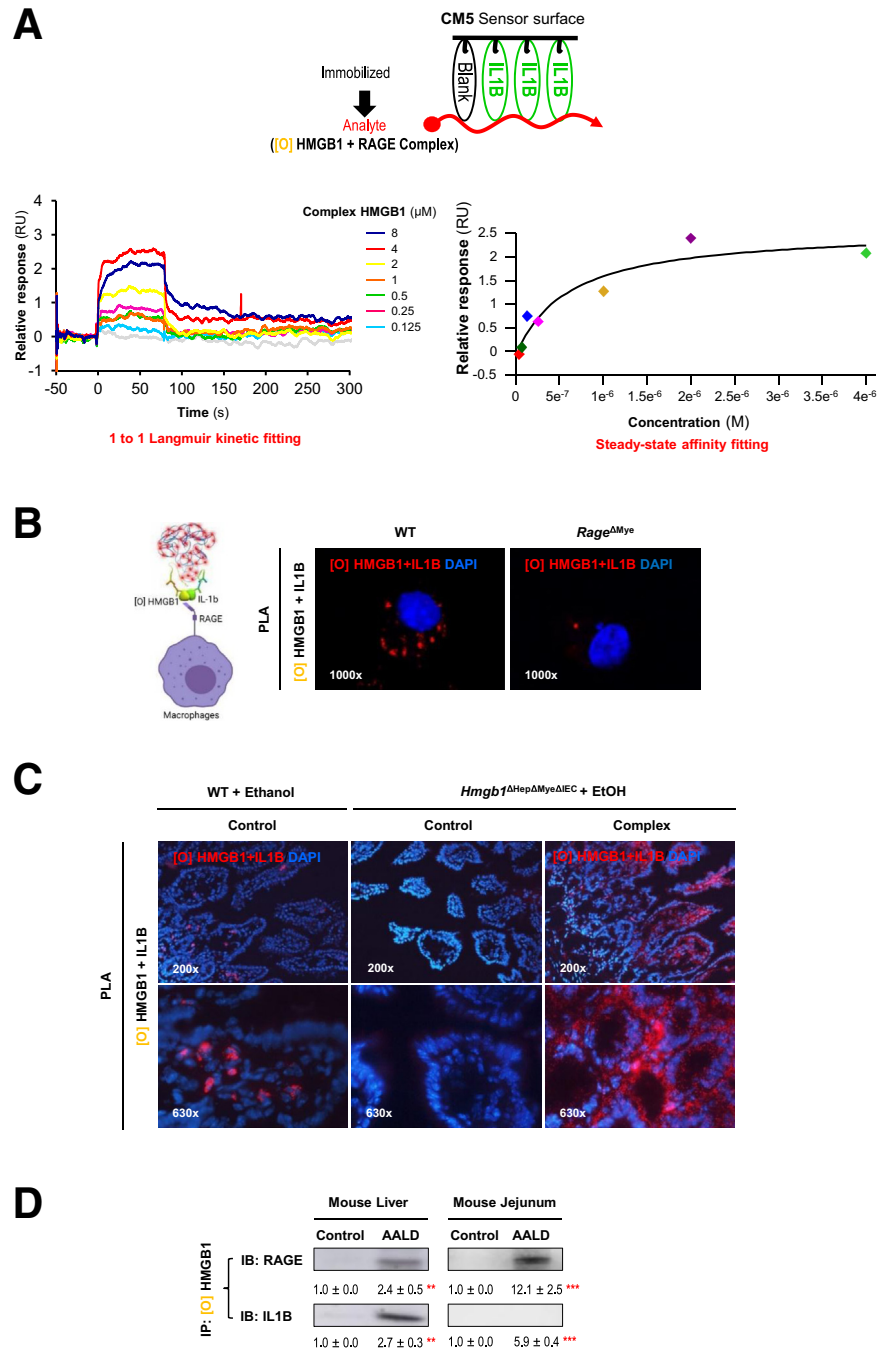
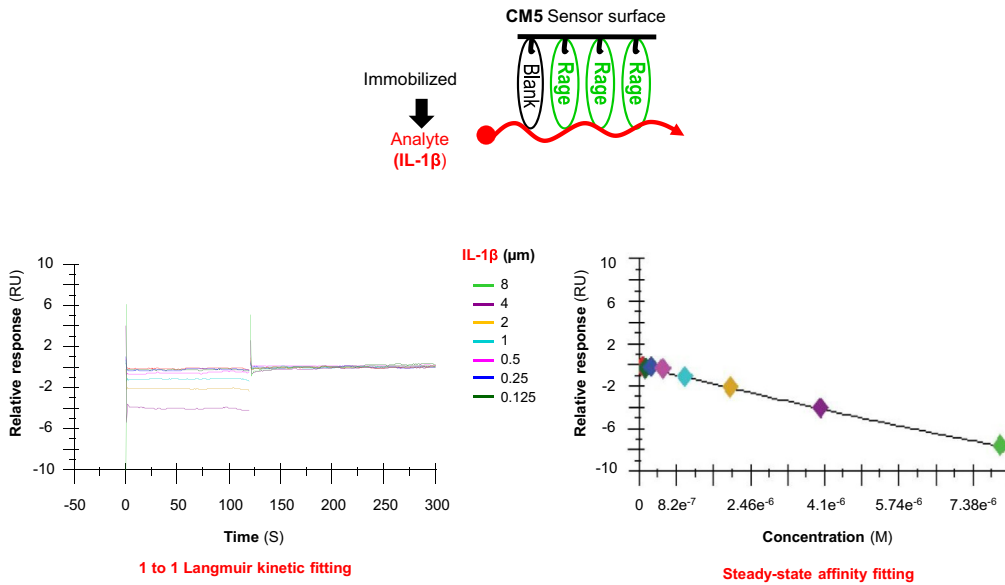


**Figure 6. The complex binds RAGE in the liver and jejunum from ethanol-fed mice.** IL-1B was captured on a CM5 sensor chip surface, and [O] HMGB1 bound to RAGE was injected at increasing concentrations for 5 minutes (A top). Sensorgrams show response at equilibrium plotted against time (A bottom left) and concentration (A bottom right). PLAs of the complex in MFs isolated from WT (controls) and *Rage*<sup>ΔMye</sup> mice (red: complex bound to RAGE) (B). PLAs on the intestine of WT (controls) and *Hmgb1*<sup>ΔHepΔMyeΔIEC</sup> mice fed ethanol (red: indicates that the complex is present in the intestine of WT but not in mice unable to produce [O] HMGB1) (C). Pull-down assays show binding of the complex to RAGE in the liver (D left) and the jejunum (D right) of ethanol-fed mice. Results are expressed as mean ± SEM; n = 6 Healthy and n = 6 AAH. n = 3 Control and n = 3 Ethanol. \*\**P* < .01 and \*\*\**P* < .001 vs Control.

First, we demonstrated that [O] HMGB1 binds RAGE using surface plasmon resonance. Furthermore, two in vivo experiments established that [O] HMGB1 signals through RAGE in Mye to drive pathogenesis in AALD. Injection of [O] HMGB1 or overexpression of WT HMGB1, which undergoes oxidation in HEPs, showed no increase in the pro-inflammatory signature, total intestinal permeability, or portal blood LPS in *Rage*<sup>ΔMye</sup> mice compared with controls. Although these studies revealed that [O] HMGB1 signals through RAGE in Mye, the possibility that complexing of [O] HMGB1 with other proteins induced in

AALD could provide a more potent stimulus for RAGE remained unknown.

Second, we revealed that HEP-derived [O] HMGB1 forms a complex with IL-1B, demonstrating binding in vitro in AAH patients and mice with AALD. Notably, the formation of the complex involves a large portion of the total amount of each protein in both human and mouse livers. We unveil that this novel complex is more potent than each component. Furthermore, we determined the complex's  $K_a$ ,  $K_d$ , and  $K_D$  constants, which allowed us to conclude that the complex is stable and has a strong affinity between proteins. Because



HEPs are the sole source of [O] HMGB1 and activated KCs and infiltrated MFs are the main hepatic source of IL-1B in AALD,<sup>6,7</sup> most of the complex likely is of liver origin. Mechanistically, the complex binds RAGE in KCs and MFs to induce a pro-inflammatory signature that exacerbates hepatic injury. Notably, each protein in this pro-inflammatory signature (TNFA, CCL2/3/5, CX3CL1) was previously implicated in the pathogenesis of AALD in patients,<sup>41–44</sup> attesting to the clinicopathologic relevance of the complex.

Third, this complex of liver origin was also found in jejunum from ethanol-fed mice. IECs produce HMGB1<sup>45</sup> but do not oxidize it and, therefore, cannot generate the complex (not shown). Thus, the production of the complex in the intestine is unlikely. Moreover, in a prior study, we demonstrated that ablation of *Hmgb1* in IECs does not alter intestinal permeability compared with WT mice with metabolic dysfunction-associated steatohepatitis.<sup>45</sup> Here, we show that the complex is absent from the intestine when HEPs do not produce [O] HMGB1; therefore, changes in total intestinal permeability and increased portal serum LPS do not occur. The complex may reach the intestine via the mesenteric artery.

In addition, we demonstrate that by binding RAGE in IECs and inducing the pro-inflammatory program, this complex alters TJ protein expression, increases intestinal permeability, and portal blood LPS. Consequently, intestinal barrier dysfunction enhances liver injury. Therefore, we propose a conceptually novel framework for a liver-to-gut pro-inflammatory feedback loop in AALD.

Regarding timing, it is possible that [O] HMGB1 signals through RAGE in early AALD. Then, as its concentration increases, it binds to other pro-inflammatory mediators, such as IL-1B, in the late stages of the disease or both. The complex may then magnify the pro-inflammatory program, exacerbating its effects in severe illness. Complexing [O] HMGB1 with IL-1B might enhance protein activity or extend

the half-life. Disrupting the interaction of the complex with its receptor via [O] HMGB1, IL-1B, RAGE-specific Abs, or small molecules could reduce hepatic and intestinal injury in AALD. Thus, this complex could drive sterile inflammatory responses to a self-perpetuating loop that results in chronic damage.

Because corticosteroids, the standard of care for severe AAH patients, have numerous side effects and are contraindicated for patients with renal failure or infections, targeting the complex with an Ab could be more specific, a multipurpose approach (trapping the complex and preventing the increase in pro-inflammatory cytokines), and perhaps a safer alternative (most Abs are typically well-tolerated). One of the effects of pentoxifylline, used for severe AAH when corticosteroids are contraindicated, is the inhibition of TNFA; therefore, targeting the complex or RAGE with an Ab would also block TNFA induction.

Our findings are conceptually innovative because they challenge our current knowledge of AALD in several ways. First, we unveil a novel liver-to-gut pro-inflammatory feedback loop caused by a complex of liver origin ([O] HMGB1 produced by HEPs and IL-1B by KCs and MFs). Second, it highlights the role of this complex signaling via RAGE in KCs and MFs to induce a pro-inflammatory signature (TNFA, CCL2/3/5, CX3CL1) that exacerbates hepatic injury. Third, it is possible that this complex, signaling via RAGE in intestinal MFs and IECs and inducing the pro-inflammatory program itself, alters TJ protein expression to drive intestinal barrier dysfunction.

Because this complex can enhance RAGE signaling, it emerges as a key upstream regulator and an attractive target to block. It could potentially be more effective in AALD prevention than blocking individual pro-inflammatory signals. This concept could be transformative because developing an Ab to neutralize the complex is feasible, and

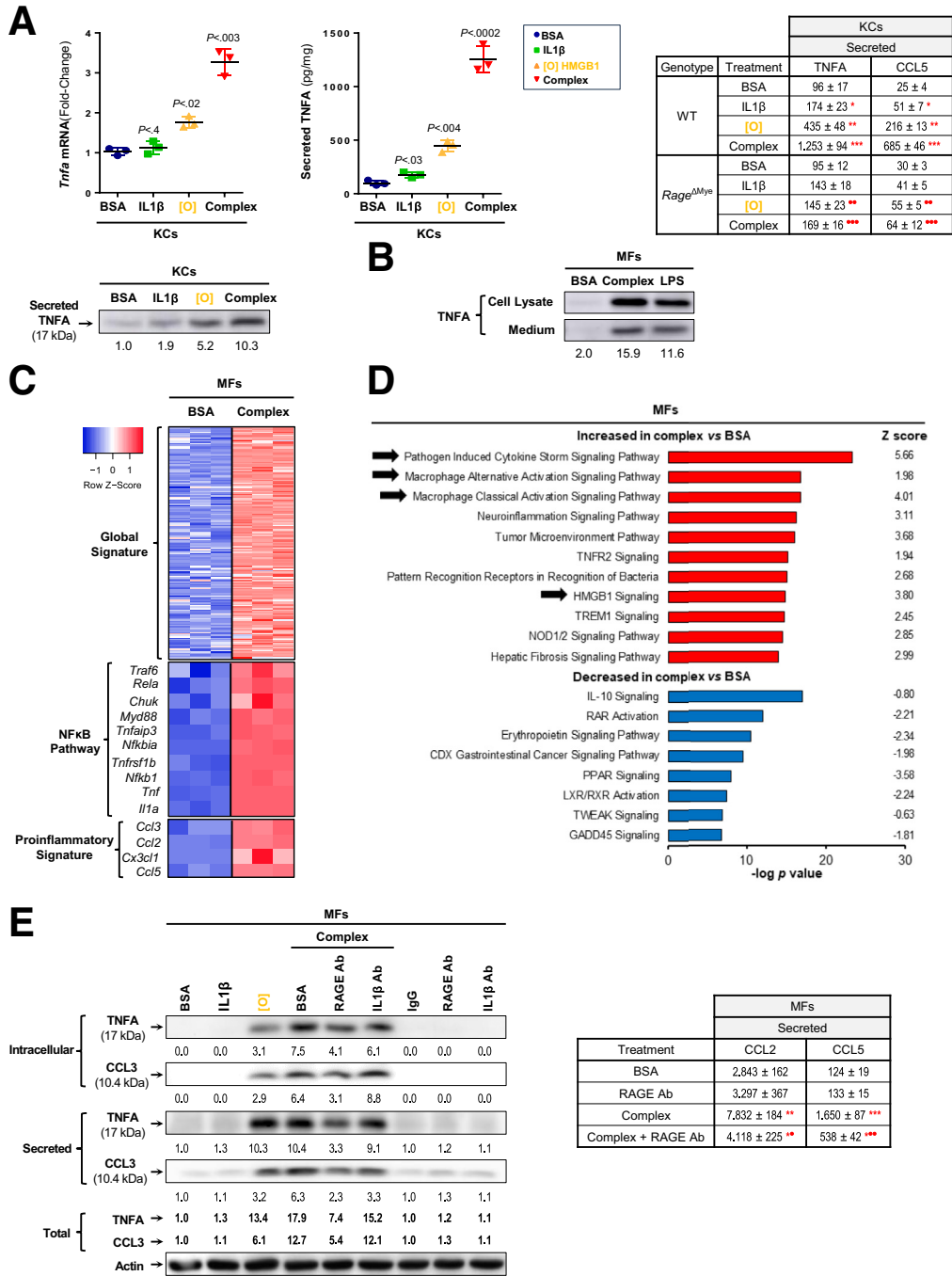
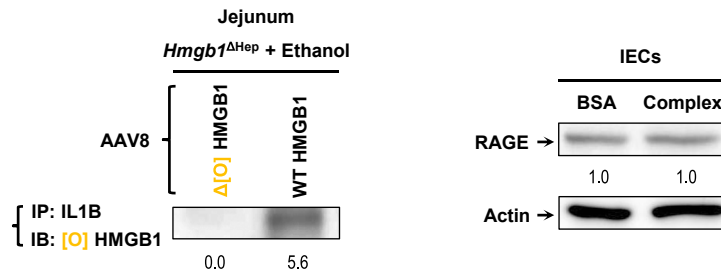


**Figure 8. The complex stimulates the production of the pro-inflammatory signature by KCs and MFs via RAGE.** qPCR for *Tnfa* mRNA (A top left), ELISA for secreted TNFA (A top middle), and Western blot for secreted TNFA (A bottom left) in primary KCs treated with IL-1B, [O] HMGB1, or the complex (all at 1 nmol/L) for 24 hours (BSA: control). Secreted TNFA and CCL5 protein in the culture medium of primary KCs from WT and *Rage*<sup>ΔMye</sup> mice treated with the complex (1 nmol/L, 12 hours) (A top right). In A and B, results are expressed as mean ± SEM; n = 3/treatment. \**P* < .05, \*\**P* < .01, and \*\*\**P* < .001 vs BSA; \*\**P* < .01 and \*\*\**P* < .001 vs WT. Western blot analysis of TNFA expression in MFs treated with 1 nmol/L of the complex or 20 nmol/L LPS (B). RNA-seq of MFs treated with the complex (1 nmol/L, 24 hours) showed activation of the same global NFκB pathway and pro-inflammatory gene signatures (C) as in livers from ethanol-fed WT (shown in Figure 1C), which were blocked in *Rage*<sup>ΔMye</sup> mice (red: up, blue: down). IPA of MFs treated with the complex (red: up, blue: down, black arrows: key pathways) (D). Western blot for intracellular and secreted TNFA and CCL3 in MFs treated with neutralizing Abs to RAGE or IL-1B (both at 10 nmol/L) 1 hour before adding the complex (1 nmol/L, 24 hours) (E left). ELISA of secreted CCL2 and CCL5 (both in pg/mg) in MFs treated with a RAGE-neutralizing Ab (10 nmol/L) 1 hour before adding the complex (1 nmol/L, 24 hours) (E right). In C–E, results are expressed as mean ± SEM; n = 3/treatment. \**P* < .05, \*\**P* < .01, and \*\*\**P* < .001 vs BSA; \**P* < .05 and \*\**P* < .01 vs Complex.

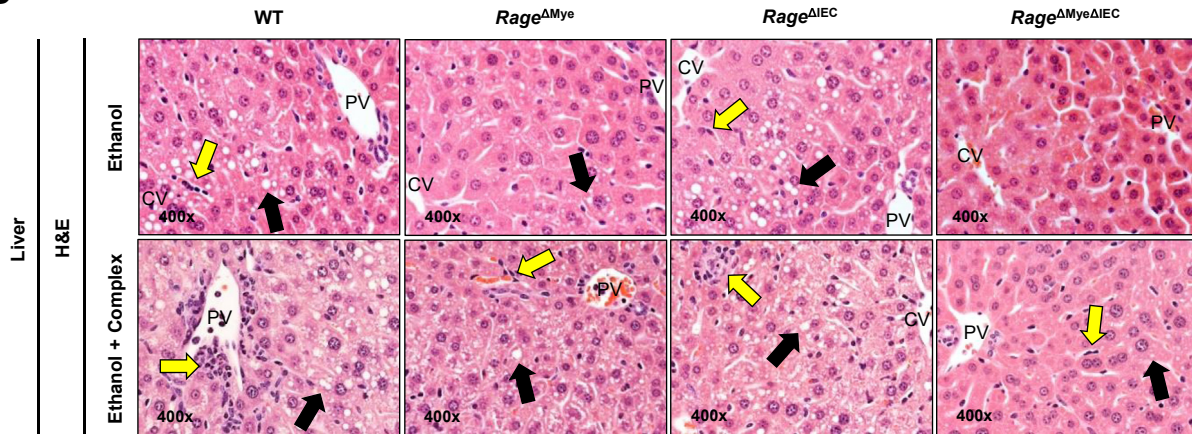
Abs against RAGE are available and safe in clinical trials; their use could have significant therapeutic potential for alcoholic patients.

Changes in this complex could be used as a biomarker of the clinical course of AALD, for treatment outcomes, and to identify patients at greater risk of progression. The notion

**A**



**B**



**C**

| Genotype                        | Treatment | Co-treatment | Histopathologic scores |                |                | Parameters of liver injury |            |             |              |
|---------------------------------|-----------|--------------|------------------------|----------------|----------------|----------------------------|------------|-------------|--------------|
|                                 |           |              | Steatosis              | Ballooning     | Inflammation   | Liver/body wt.             | Serum ALT  | Liver TG    | Mortality    |
| WT                              | Ethanol   | No           | 1.54 ± 0.14            | 1.53 ± 0.11    | 2.07 ± 0.07    | 0.042 ± 0.002              | 184 ± 25   | 228 ± 19    | 7% (1/14)    |
| <i>Rage</i> <sup>ΔMyc</sup>     |           |              | 0.73 ± 0.13 *          | 0.75 ± 0.06 *  | 1.59 ± 0.04 *  | 0.038 ± 0.002              | 92 ± 14 *  | 129 ± 21 *  | 0% (0/8) *   |
| <i>Rage</i> <sup>ΔIEC</sup>     |           |              | 1.36 ± 0.19            | 0.71 ± 0.04 *  | 1.84 ± 0.06    | 0.038 ± 0.002              | 134 ± 22   | 167 ± 16    | 0% (0/8) *   |
| <i>Rage</i> <sup>ΔMycΔIEC</sup> |           |              | 0.66 ± 0.06 **         | 0.48 ± 0.04 *  | 1.42 ± 0.06 *  | 0.036 ± 0.002 *            | 77 ± 12 *  | 132 ± 14 *  | 0% (0/8) *   |
| WT                              | Ethanol   | Complex      | 1.74 ± 0.22            | 1.42 ± 0.12    | 2.55 ± 0.08 *  | 0.051 ± 0.002              | 267 ± 39 * | 293 ± 38    | 25% (2/8) *  |
| <i>Rage</i> <sup>ΔMyc</sup>     |           |              | 0.58 ± 0.12 **         | 0.64 ± 0.08 ** | 1.54 ± 0.09 ** | 0.042 ± 0.001 *            | 102 ± 14 * | 136 ± 20 ** | 0% (0/8) **  |
| <i>Rage</i> <sup>ΔIEC</sup>     |           |              | 1.21 ± 0.08 *          | 1.36 ± 0.16 *  | 2.11 ± 0.12 ** | 0.041 ± 0.003 *            | 164 ± 21 * | 149 ± 12 *  | 25% (2/8) ** |
| <i>Rage</i> <sup>ΔMycΔIEC</sup> |           |              | 0.55 ± 0.04 **         | 0.57 ± 0.04 ** | 1.38 ± 0.03 ** | 0.038 ± 0.002 **           | 81 ± 13 ** | 122 ± 10 ** | 0% (0/8) **  |

**D**

| Genotype                        | Treatment | Co-treatment | Proinflammatory signature (liver) |            |            |                |           |
|---------------------------------|-----------|--------------|-----------------------------------|------------|------------|----------------|-----------|
|                                 |           |              | TNFA                              | CCL2       | CCL3       | CCL5           | CX3CL1    |
| WT                              | Ethanol   | No           | 271 ± 27                          | 178 ± 22   | 106 ± 13   | 3.714 ± 162    | 40 ± 5    |
| <i>Rage</i> <sup>ΔMyc</sup>     |           |              | 165 ± 24 *                        | 95 ± 16 *  | 65 ± 7 *   | 2.527 ± 105 *  | 23 ± 4 *  |
| <i>Rage</i> <sup>ΔIEC</sup>     |           |              | 229 ± 31                          | 124 ± 23   | 74 ± 11    | 3.183 ± 136    | 34 ± 6    |
| <i>Rage</i> <sup>ΔMycΔIEC</sup> |           |              | 140 ± 19 *                        | 57 ± 12 ** | 42 ± 6 **  | 2.245 ± 94 *   | 26 ± 4 *  |
| WT                              | Ethanol   | Complex      | 387 ± 52 *                        | 272 ± 32 * | 195 ± 27 * | 4.937 ± 195 *  | 95 ± 8 *  |
| <i>Rage</i> <sup>ΔMyc</sup>     |           |              | 178 ± 31 *                        | 121 ± 24 * | 72 ± 9 *   | 3.182 ± 158 *  | 31 ± 7 ** |
| <i>Rage</i> <sup>ΔIEC</sup>     |           |              | 265 ± 46                          | 139 ± 12 * | 89 ± 13 *  | 3.985 ± 149    | 57 ± 9    |
| <i>Rage</i> <sup>ΔMycΔIEC</sup> |           |              | 147 ± 22 **                       | 65 ± 14 ** | 51 ± 15 ** | 2.769 ± 127 ** | 35 ± 5 *  |

that this complex exacerbates hepatic injury and is a retrograde mechanism whereby the liver enhances intestinal permeability adds a new pro-inflammatory feedback loop to drive the progression of AALD.

Our work underscores the complex but specific mechanisms through which HMGB1 isoforms influence liver disease outcomes. Previously, we showed that [O] HMGB1 induces hepatic stellate cell activation, thereby exacerbating liver fibrosis, whereas sulfonated HMGB1 induces apoptosis in hepatic stellate cells, contributing to fibrosis regression.<sup>46</sup> The current study delineates a novel pro-inflammatory mechanism mediated by [O] HMGB1 through its interaction with RAGE on KCs and MFs in AALD. This interaction triggers a local inflammatory cascade within the liver that extends to the intestine. Moreover, [O] HMGB1 forms a potent complex with IL-1B, further intensifying the inflammatory response. This complex exhibits a specific affinity for RAGE within the liver and across intestinal MFs and IECs, precipitating adverse effects. Thus, the dual role of RAGE as a signaling mediator in both liver fibrosis and AALD pathogenesis is noteworthy. Although its activation in hepatic stellate cells is pivotal for fibrosis progression, RAGE activation in KCs and MFs emerges as a critical factor in exacerbating AALD.

There are some limitations in our study. Although restorative macrophages are involved in liver repair after injury, we used a model of early alcohol-induced liver injury, not of resolution. In addition, KCs and infiltrating MFs each play distinct yet interconnected roles in liver homeostasis and pathology, including AALD. It is possible to use genetic models with specific *Cre* recombinase lines to dissect the roles of these cell populations in the liver's response to injury. Such strategies could offer valuable insights but are accompanied by inherent limitations, including the specificity of *Cre* expression and potential compensatory mechanisms that might obscure the direct effects of gene deletion. As for how to compare the effect of monocyte-derived MFs with intestinal Mye, this remains a challenge. The intestinal-liver axis, pivotal in conditions such as AALD, involves a complex interplay of barrier integrity, microbial translocation, and immune activation that complicates the isolation of specific cellular contributions. To advance our understanding in this field, innovative experimental designs are needed. For example, using dual-reporter mice or adoptive transfer experiments with genetically tagged cells could provide insights into the dynamics of cell trafficking and function. In addition, advanced imaging techniques, single-cell sequencing, and cell trajectory analyses might

offer unprecedented resolution in distinguishing the roles and origins of MF populations within diseased tissues.

## Materials and Methods

### General Methodology

Details on general methods such as serum ALT activities, liver triglycerides, H&E staining, IHC, Western blot analysis, mRNA isolation, and qPCR are described in our previous publications.<sup>5,24,34,47-49</sup>

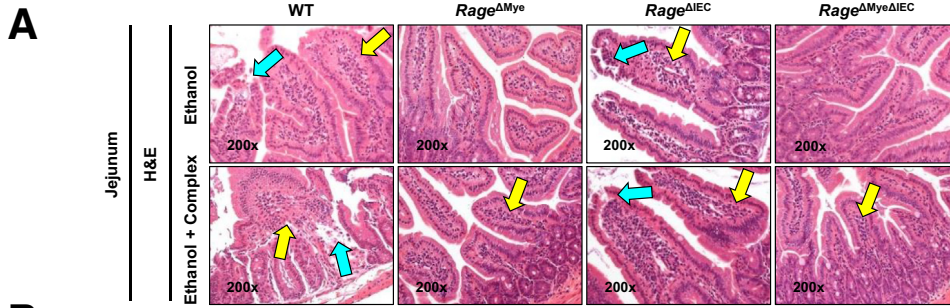
### Antibodies and Enzyme-linked Immunosorbent Assay Kits

Abs used in Western blot analysis were sourced from various suppliers: HMGB1 (sc-56698), RAGE (sc-365154), and actin (sc-1616) were obtained from Santa Cruz Biotechnology (Santa Cruz, CA); TNFA (70R-TR008) from Fitzgerald (Acton, MA); IL-1B (AF-401-NA) from R&D Systems (Minneapolis, MN); CCL3 (ab179638) and CLDN7 (ab27487) from Abcam (Cambridge, MA); ZO-1 (PA5-28858), OCLN (711500), CLDN2 (51-6100), and CLDN5 (34-1600) from Invitrogen (Carlsbad, CA). HMGB1 (ab18256) and IL-1B (ab9722) from Abcam were used in pull-down assays. Electrophoresis was performed under non-reducing or reducing conditions to detect [O] HMGB1. Enzyme-linked immunosorbent assay (ELISA) kits were used to determine TNFA (EK0525, Boster Biological), CX3CL1 (RAB0113, Sigma-Aldrich, St Louis, MO), and CCL2 (BMS281), CCL3 (88-56013), and CCL5 (KMC1031), all from Invitrogen (Waltham, MA).

### Mice

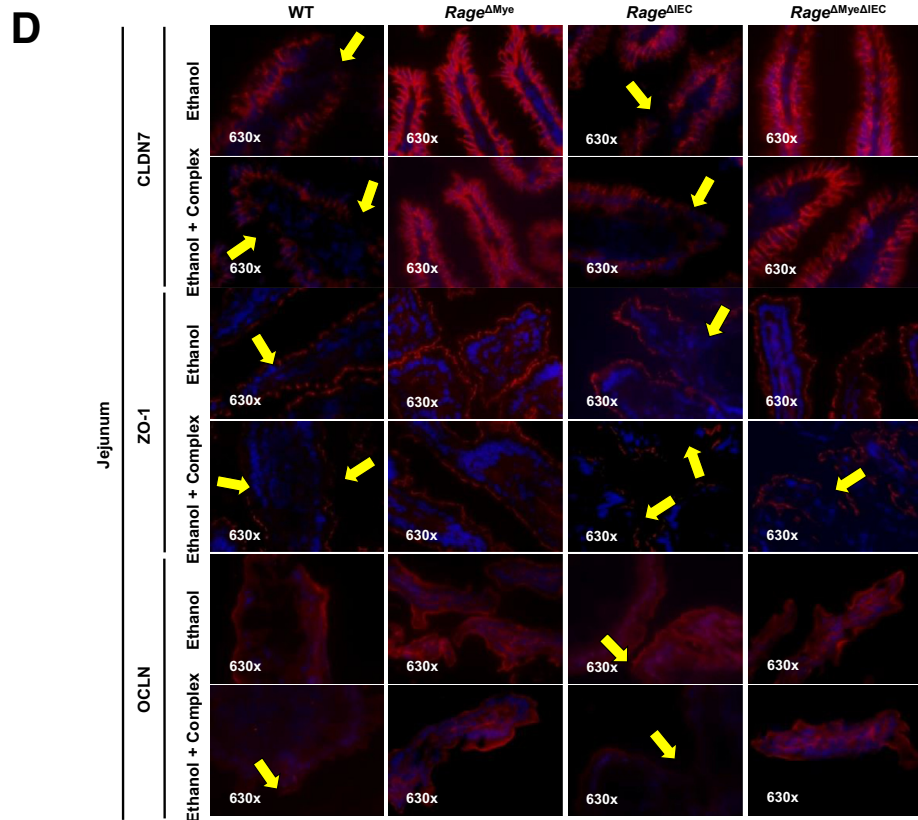
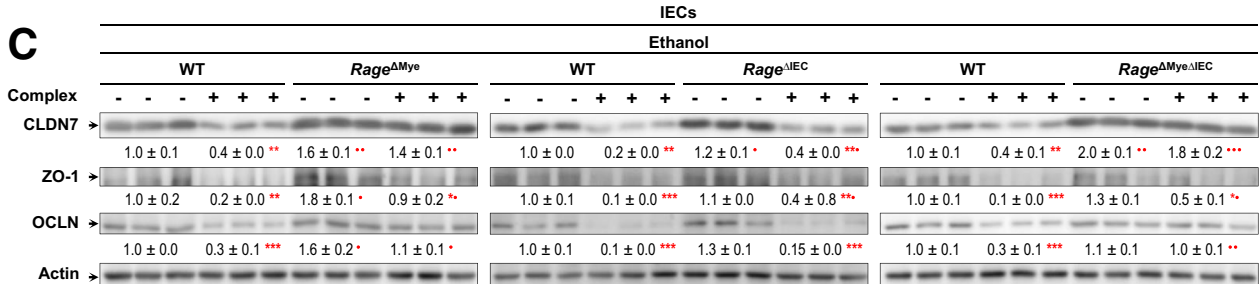
*Hmgb1*<sup>fl/fl</sup> mice were donated by Dr Timothy R. Billiar (University of Pittsburgh, Pittsburgh, PA). The *Hmgb1*<sup>loxP</sup> allele was created by inserting *loxP* sites within introns 1 and 2 and flanking exon 2 of *Hmgb1* [39]. *Rage*<sup>fl/fl</sup> mice were obtained from Dr Bernd Arnold (German Cancer Research Center, Heidelberg, Germany). The *Rage*<sup>loxP</sup> allele was created by inserting *loxP* sites flanking exons 2-7 of *Rage*.<sup>50</sup> *Tlr4*<sup>fl/fl</sup> mice were a gift from Dr David J. Hackam (University of Pittsburgh, Pittsburgh, PA). The *Tlr4*<sup>loxP</sup> allele was created by inserting *loxP* sites flanking exon 2 of *Tlr4*.<sup>51</sup> Floxed mice were bred with *Albumin.Cre* (JAX:003574, B6.Cg-Tg(Alb-cre)21Mgn/J), *Lysozyme-2 (Lyz2).Cre* (JAX:004781, B6.129P2-*Lyz2*<sup>tm1(cre)Jfo</sup>/J), or *Villin (Vil).Cre* (JAX:004586, B6.Cg-Tg(Vil1-cre)997Gum/J) (Jackson Laboratory, Bar Harbor, ME) to generate HEP-specific, Mye-specific, IEC-specific, and

**Figure 9.** (See previous page). **The complex is absent in the intestine when HEPs do not produce [O] HMGB1.** Pull-down assay demonstrating the presence of the complex in jejunum from ethanol-fed *Hmgb1*<sup>ΔHep</sup> mice expressing WT but not Δ[O] HMGB1 (A left). Western blot analysis of RAGE in primary IECs treated with the complex (A right). The complex binds RAGE in myeloid cells and IECs to increase hepatic inflammation and intestinal permeability and enhance portal blood LPS in AALD. WT (controls), *Rage*<sup>ΔMye</sup>, *Rage*<sup>ΔIEC</sup>, and *Rage*<sup>ΔIECΔMye</sup> mice were injected with the complex while being fed an ethanol LDC diet for 6 weeks. Liver H&E staining (black arrows: steatosis, yellow arrows: inflammation) (B). Histopathologic scores (steatosis, hepatocyte ballooning degeneration, inflammation), parameters of liver injury (liver-to-body weight ratios, serum ALT activities, liver triglycerides), and mortality rates (C). Liver pro-inflammatory signature (TNFA, CCL2, and CCL5 are in pg/mg, CCL3 and CX3CL1 are in ng/mg) (D). Results are expressed as mean ± SEM; n = 6 male and n = 6 female/group; \*P < .05 and \*\*P < .01 vs WT. •P < .05 and ••P < .01 vs no complex.



**B**

| Parameters of intestinal injury |           |              |                               |                  |                    |
|---------------------------------|-----------|--------------|-------------------------------|------------------|--------------------|
| Genotype                        | Treatment | Co-treatment | Total intestinal permeability | Portal blood LPS | Pathological score |
| WT                              | Ethanol   | No           | 1.397 ± 145                   | 145 ± 9          | 2.6 ± 0.2          |
| <i>Rage</i> <sup>ΔMyc</sup>     |           |              | 976 ± 102 *                   | 102 ± 7 *        | 1.1 ± 0.1 **       |
| <i>Rage</i> <sup>ΔIEC</sup>     |           |              | 1.253 ± 94                    | 124 ± 15         | 2.3 ± 0.1          |
| <i>Rage</i> <sup>ΔMycΔIEC</sup> |           |              | 827 ± 75 *                    | 83 ± 8 *         | 1.0 ± 0.1 **       |
| WT                              | Ethanol   | Complex      | 2.478 ± 224 *                 | 295 ± 37 **      | 3.7 ± 0.4 *        |
| <i>Rage</i> <sup>ΔMyc</sup>     |           |              | 1.265 ± 138 *                 | 143 ± 12 *       | 1.4 ± 0.2 **       |
| <i>Rage</i> <sup>ΔIEC</sup>     |           |              | 1.636 ± 129 **                | 180 ± 14 **      | 2.8 ± 0.2 *        |
| <i>Rage</i> <sup>ΔMycΔIEC</sup> |           |              | 1.083 ± 102 **                | 114 ± 16 **      | 1.3 ± 0.3 **       |



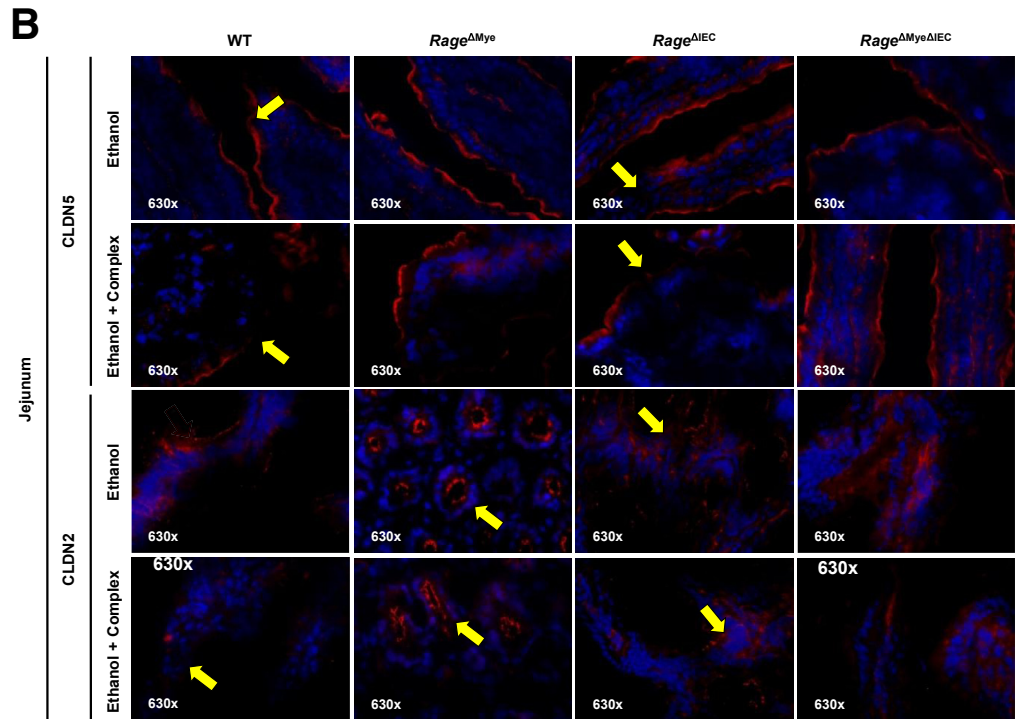
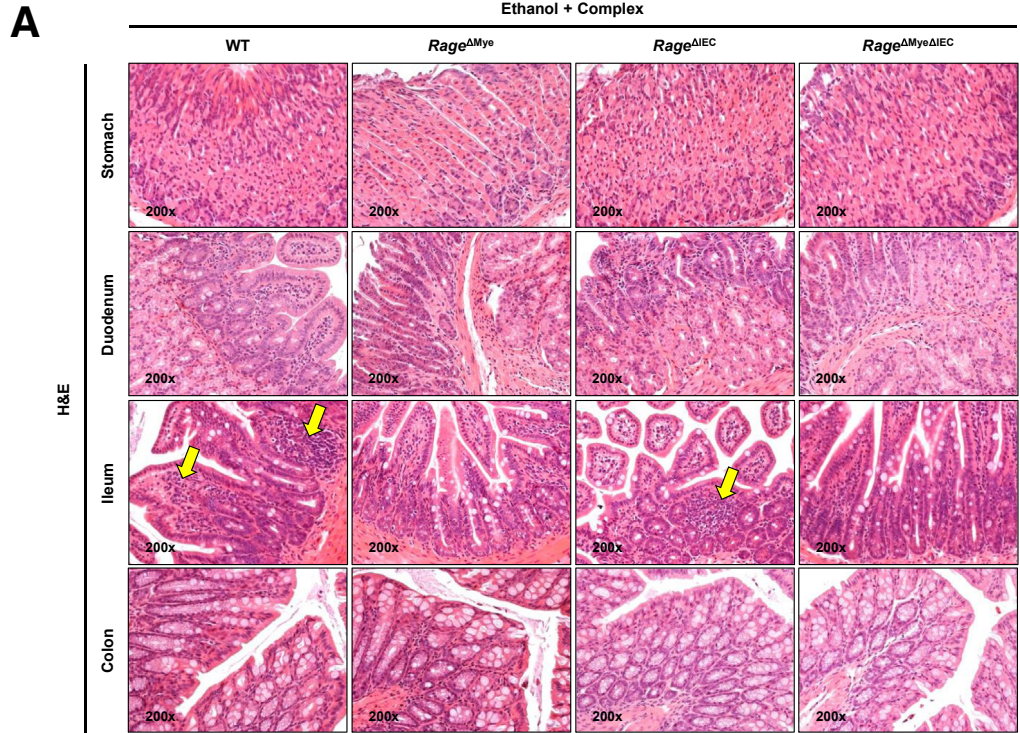


**Figure 11. The complex alters tight junction protein expression.** WT (controls), *Rage*<sup>ΔMyc</sup>, *Rage*<sup>ΔIEC</sup>, and *Rage*<sup>ΔIECΔMyc</sup> mice were injected with the complex while being fed an ethanol LDC diet for 6 weeks. Stomach, duodenum, ileum, and colon H&E staining (yellow arrows: inflammation) (A). Immunofluorescence for CLDN5 and CLDN2 in jejunum (yellow arrows: positive staining) (B). n = 6 male and n = 6 female/group.

**Figure 10. (See previous page). The complex alters IEC tight junction protein expression.** WT (controls), *Rage*<sup>ΔMyc</sup>, *Rage*<sup>ΔIEC</sup>, and *Rage*<sup>ΔIECΔMyc</sup> mice were injected with the complex while being fed an ethanol LDC diet for 6 weeks. Jejunum H&E staining (yellow arrows: inflammation, blue arrows: focal ulceration) (A). Parameters of intestinal injury (total intestinal permeability [FITC fluorescence units], portal blood LPS [pg/mL], pathologic scores) (B). Western blot for CLDN7, ZO-1, and OCLN in IECs isolated from these mice (C). Immunofluorescence for CLDN7, ZO-1, and OCLN in jejunum from these mice (yellow arrows: positive staining) (D). Results are expressed as mean ± SEM; n = 6 male and n = 6 female/group. \*P < .05, \*\*P < .01, and \*\*\*P < .001 vs WT. •P < .05, ••P < .01, and •••P < .001 vs no complex.

combinations thereof of conditional knockout mice. Thus, the mouse lines generated for this study were *Hmgb1*<sup>ΔHep</sup>, *Hmgb1*<sup>ΔHepΔMycΔIEC</sup>, *Hmgb1&Rage*<sup>ΔHepΔMyc</sup>, *Rage*<sup>ΔIEC</sup>, *Rage*<sup>ΔIECΔMyc</sup>, *Rage*<sup>ΔMyc</sup>, and *Tlr4*<sup>ΔMyc</sup> mice. Controls, referred to WT, were used in all experiments. First, each *Cre* mouse line that had not been crossed to any *fl/fl* mouse line was used as a control for *Cre*-induced recombination at cryptic *lox* sites in the genome. Second, each *fl/fl* mouse line that had not been crossed to any *Cre* mouse line was used as a control for the effects of introducing *loxP* sites into the intron regions of the gene of interest. All *loxP*-flanked (floxed) strains were re-derived using C57BL/6J oocytes donors. All mice lacked a liver phenotype in the absence of any treatment.

### Model of Alcohol-induced Liver Injury

The LDC model was used to provoke early alcohol-induced liver injury. Control and ethanol LDC diets (Bio-Serv Inc, Frenchtown, NJ) are equicaloric and have the same composition concerning fat (42% of calories) and protein (16% of calories). The content of carbohydrates is 42% of total calories (dextrin-maltose) in the control diet and 12% in the ethanol diet, where up to 30% of carbohydrate calories are replaced by ethanol.<sup>52</sup> To determine the contribution of the cell source of HMGB1 and the involvement of RAGE and TLR4 signaling in AALD, an equal number ( $n = 6$ /sex/condition) of 10-week-old male and female *Hmgb1*<sup>ΔHep</sup>, *Hmgb1*<sup>ΔHepΔMyc</sup>, *Hmgb1*<sup>ΔHepΔMycΔIEC</sup>, *Hmgb1&Rage*<sup>ΔHepΔMyc</sup>, *Rage*<sup>ΔIEC</sup>, *Rage*<sup>ΔMyc</sup>, *Rage*<sup>ΔIECΔMyc</sup>, *Tlr4*<sup>ΔMyc</sup>, and their corresponding control mice were used with the LDC model for 6 weeks. Mice were acclimatized to the liquid diet by feeding them the control diet for 3 days. The percentage of ethanol-derived calories progressively increased from 10% (1 week) to 20% (1 week), 25% (2 weeks), and 30% (~2 weeks). Mice were pair-fed, and liver and body weights were logged on death to calculate the liver-to-body weight ratios. We use the littermate approach to control genetic and environmental background. Mice are randomly chosen from several cages and randomly assigned to each treatment group to avoid the batch effect. Blood was collected by submandibular bleeding under anesthesia, and livers were removed for further analysis.

To explore the role of [O] HMGB1 and RAGE signaling in AALD, an equal number ( $n = 6$ /sex/condition) of 10-week-old male and female WT (controls) and *Rage*<sup>ΔMyc</sup> mice were injected intraperitoneally with BSA, [H] HMGB1 (1690-HM, R&D Systems), or [O] HMGB1 (cat. no. 211009, IBL International), at a dose of 0–0.1 μg/g,<sup>33</sup> throughout the ethanol feeding protocol. To further validate the role of [O] HMGB1 in AALD, an equal number ( $n = 6$ /sex/condition) of 10-week-old male and female *Hmgb1*<sup>ΔHep</sup> and *Hmgb1&Rage*<sup>ΔHepΔMyc</sup> mice were transduced with AAV8 vectors, containing the *Tbg* promoter, to target HEPs specifically.<sup>53,54</sup> The vectors were AAV8.*Tbg.WT.Hmgb1.Gfp*, to overexpress native or WT HMGB1 that can undergo post-translational modifications, and AAV8.*Tbg.NLS1(2C→2S).Gfp* that cannot produce [O] HMGB1 (Δ[O] HMGB1). Two weeks after successful expression, mice were fed the LDC diets. A

final experiment was performed with *Rage*<sup>ΔMyc</sup>, *Rage*<sup>ΔIEC</sup>, *Rage*<sup>ΔIECΔMyc</sup>, and their corresponding control mice, where the complex was injected intraperitoneally at a dose of 4 pmol/L/g twice a week during the ethanol-feeding experiment.

### Gut Permeability

Mice were gavaged with 100 μL FITC-dextran 4 (Sigma-Aldrich) (160 mg/kg) under fasting conditions 4 hours before euthanization. FITC-dextran-4 fluorescence was quantified in portal blood serum and expressed as total intestinal permeability adjusted by the volume of the clean intestine. Portal blood LPS was measured using the chromogenic LAL assay from Lonza Inc (Allendale, NJ).

### Pathology

In all experiments, we collected the entire left liver lobe from all mice, and intestinal Swiss rolls were prepared. Tissues were fixed in 4% neutral-buffered formalin and sectioned into 4-μm paraffin sections for H&E staining. Steatosis grade was 0 = <5%, 1 = 5%–33%, 2 = >33%–66%, and 3 = >66%. Scores for necrosis were 1 = hepatocyte necrosis affecting only zone 3, 2 = in addition to zone 3 necrosis, occasional bridging necrosis was seen, and 3 = pronounced bridging and confluent necrosis. In the LDC model, necrosis is minimal regardless of genotype. Ballooning degeneration was identified when HEPs were enlarged, in most cases, to more than twice the size of their neighboring cells. In addition, the cytoplasmic membrane became rounded instead of the usual hexagonal shape of normal HEPs. Most of the cytoplasm appeared empty, except for a few irregular wisps of pink material, representing damaged cytoplasmic content. Inflammation was noted to be lymphocytes present in lobules and was scored as 1 = rare foci, 2 = up to 5 foci, and 3 when there were >5 foci. Pathologic scoring of intestinal segments was as follows: 1 = mild mucosal inflammatory cell infiltrates with intact epithelium, 2 = moderate inflammatory cell infiltration into the mucosa with intact epithelium, 3 = mucosal infiltrates with focal ulceration, and 4 = mucosal infiltrates with extensive ulceration.<sup>55</sup> The assessment of the above scores was uniformly performed under ×200 magnification.

### Cells and Treatment

Primary KCs were isolated from control and *Rage*<sup>ΔMyc</sup> mice as previously shown.<sup>56,57</sup> Cells were treated with serum-free Dulbecco modified Eagle medium-F12 before treatment with IL-1B, [O] HMGB1, and the [O] HMGB1 + IL-1B complex (all at 1 nmol/L) for 24 hours. Cell lysate and culture medium were collected for protein or mRNA analysis. Raw 264.7 MFs were seeded (10,000 cells/well) on 12-well plates in Dulbecco modified Eagle medium/F12 with 10% fetal bovine serum. Cells were cultured using Dulbecco modified Eagle medium-F12 for 1 day. The medium was replaced by serum-free Dulbecco modified Eagle medium-F12 before treatment with IL-1B, [H] HMGB1, [O] HMGB1, [H] HMGB1 + IL-1B, and [O] HMGB1 + IL-1B (all at 1 nmol/L) for 24 hours. To prepare the complex, equal HMGB1 and



IL-1B were bound in a tube at 37°C for 30 minutes and added to the cells. To compare the effects of the complex with those from LPS, MFs were treated with the [O] HMGB1 + IL-1B complex (1 nmol/L) or LPS (2 nmol/L) for 24 hours. To determine whether the effects of the complex were RAGE-dependent, MFs were co-treated with neutralizing Abs to RAGE or IL-1B or non-immune rabbit immunoglobulin G at a dose of 5 nmol/L, respectively, for 24 hours. Cell lysate and culture medium were collected for protein analysis or RNA sequencing. IECs were isolated from WT (controls), *Rage*<sup>ΔMye</sup>, and *Rage*<sup>ΔIEC</sup> mice, as previously shown,<sup>45</sup> and immediately used for protein analysis.

### In Vitro Reconstituted System

Binding of [H] HMGB1 or [O] HMGB1 to IL-1B was analyzed by incubating [H] HMGB1, [O] HMGB1, or IL-1B (all at 1.5 nmol/L), alone or with neutralizing Abs to HMGB1 or IL-1B or non-immune immunoglobulin G, for 1 hour at 37°C. In pull-down assays, HMGB1 (ab18256) and IL1B (ab9722) from Abcam were used. For the Western blot, IL-1B (AF-401-NA) was from R&D systems and HMGB1 (sc56698) from Santa Cruz.

### Surface Plasmon Resonance

To assess the binding of [O] HMGB1 (analyte) to RAGE (ligand), RAGE was captured on a CM5 sensor chip surface, and [O] HMGB1 was added in serial dilutions to the buffer flowing over the ligand surface. To analyze the formation of the complex, IL-1B was captured on a CM5 sensor chip surface, and its potential binders ([H] HMGB1 and [O] HMGB1) were injected. To determine the binding of the complex to RAGE, IL-1B was captured on a CM5 sensor chip surface, and the complex of [O] HMGB1 and RAGE was injected. The composition of the binding buffer used was 10 mmol/L HEPES pH 7.4, 150 mmol/L NaCl, 3 mmol/L EDTA, 0.05% Tween P20, and 0.1% BSA. Real-time interaction between the analytes and their ligands was monitored on a Biacore 8K (Cytiva, Marlborough, MA) as a change in refractive index over time. The multi-cycle assay conditions were 100 seconds of association, 300 seconds of dissociation, 30 μL/min of flow rate, and 25°C. The analytes were injected at 0–10 μmol/L for 5 minutes to generate the sensorgrams. The association rate ( $k_a$ ), dissociation rate ( $k_d$ ), and equilibrium dissociation ( $K_D$ ) constants were calculated. Data were fit to the Langmuir kinetic binding model, which describes a 1:1 interaction where one ligand molecule interacts with one analyte molecule by steady-state affinity. The responses at equilibrium were plotted against time and concentration.

### PLA Staining

Primary KCs were isolated from *Rage*<sup>ΔMye</sup> and WT mice livers with anti-F4/80 microbeads (130-110-443, Miltenyi Biotec, San Diego, CA) and were cultured overnight. Cells were blocked with IL1R Ab (MAB4801, Bio-technie, Minneapolis, MN) for 2 hours, washed, bound with the complex of [O] HMGB1 with IL-1B (both at 5 nmol/L) for 2 hours, and then fixed with 4% paraformaldehyde. They were blocked with

Dako protein block (X0909, Agilent, Santa Clara, CA) for 60 minutes, bound with a mix of antibodies against HMGB1 and IL-1B overnight at 4°C. The PLA staining was done with Duolink in situ red start kit reagents (Duo92103, Sigma-Aldrich). Briefly, the plus and minus PLA probes were added to cells and incubated for 1 hour at 37°C. The ligation was performed with ligase for 30 minutes, and the amplification with polymerase was carried out for 100 minutes. Slides were mounted with an in situ mounting medium with DAPI.

### AAV8 Viral Vectors

The constructs to engineer the AAV8 vectors were *Tbg.N1.Gfp*, as negative control; *Tbg.WT.Hmgb1.Gfp*, with nuclear localization signals 1/2 to overexpress native HMGB1 that can undergo post-translational modifications; and *Tbg.NLS1(2C→2S).Gfp*, to generate Δ[O] HMGB1, as cysteines 23 and 45 in the nuclear localization signal-1 are mutated to serines and cannot be oxidized. Cloning and construction of the AAV8 vectors, large-scale preparation, and quality control were carried out by the University of Pennsylvania Vector Core (Philadelphia, PA). To determine whether the AAV8 viral vectors encoding WT or mutated *Hmgb1* conferred adequate HMGB1 expression and localization in mice, a pilot experiment was performed by administering systemically via the tail vein a single dose of the vectors (1-3e<sup>11</sup> genome copies/mouse in 100 μL of sterile saline solution) to *Hmgb1*<sup>ΔHepΔMye</sup> mice for ease of HMGB1 visualization (n = 4, 8-week-old mice/vector). Maximal expression occurred 2 weeks after vectors' injections, and transduction efficiency was determined by quantification of green fluorescent protein fluorescence or HMGB1 IHC.

### Transcriptome Profiling

Liver and MFs mRNA were extracted using the Illustra RNAspin Mini Kit (GE Healthcare Bio-Sciences, Pittsburgh, PA). RNA libraries were prepared for sequencing using standard protocols, and global transcriptome profiling was performed by RNA-seq. The 100-nucleotide single-end sequencing was done on a HiSeq 2000 (Illumina, San Diego, CA). Transcript expression levels were quantified as transcripts per kilobase million using the TopHat and Cufflinks applications from BaseSpace (Illumina).<sup>58</sup>

Differentially expressed molecular pathways were surveyed using GSEA 16 on a comprehensive gene set collection available at the Molecular Signatures Database (Broad Institute, Boston, MA) for bioinformatics analysis. Genes in the genome-wide transcriptome profiles were ranked according to the differential expression between the experimental groups based on *t* statistics. Predefined gene sets annotated by biological function in the Molecular Signatures Database were mapped onto the gene list. The distribution of each gene set as up- or down-regulated was quantitatively evaluated using Kolmogorov-Smirnov statistics. Significance was determined based on the null distribution of the statistics, iteratively calculated by random permutation of gene IDs 1000 times and adjusted for multiple hypothesis testing by false discovery rate. When a fold discovery rate

was  $<0.25$ , it was considered statistically significant. IPA (Qiagen Bioinformatics, Redwood City, CA) was used to determine molecular interactions and perform pathway enrichment analysis.

### Study Approvals

All animals received humane care according to criteria outlined in the Guide for the Care and Use of Laboratory Animals, prepared by the National Academy of Sciences and published by the National Institutes of Health. The University of Illinois at Chicago IACUC office approved housing and husbandry conditions before initiating the studies. All in vivo experiments were carried out according to ARRIVE guidelines. Liver samples from healthy volunteers and patients with moderate or severe AAH naive to treatment were provided by the University of Illinois at Chicago Tissue Biorepository on approval of the request by the Institutional Review Board.

### Statistical Analysis

Data are expressed as mean  $\pm$  standard error of the mean (SEM). Statistical comparisons between groups and treatments in vitro were performed using paired Student *t* test, and experiments were performed in triplicate. In vivo data were analyzed using a two-factor analysis of variance.

### References

- O'Shea RS, Dasarthy S, McCullough AJ, et al. Alcoholic liver disease. *Hepatology* 2010;51:307–328.
- Crabb DW, Bataller R, Chalasani NP, et al. Standard definitions and common data elements for clinical trials in patients with alcoholic hepatitis: recommendation from the NIAAA Alcoholic Hepatitis Consortia. *Gastroenterology* 2016;150:785–790.
- Ambade A, Mandrekar P. Oxidative stress and inflammation: essential partners in alcoholic liver disease. *International Journal of Hepatology* 2012;2012:853175.
- Mandrekar P, Szabo G. Signalling pathways in alcohol-induced liver inflammation. *J Hepatol* 2009;50:1258–1266.
- Ge X, Antoine DJ, Lu Y, et al. High mobility group box-1 (HMGB1) participates in the pathogenesis of alcoholic liver disease (ALD). *J Biol Chem* 2014;289:22672–22691.
- McClain CJ, Cohen DA, Dinarello CA, et al. Serum interleukin-1 (IL-1) activity in alcoholic hepatitis. *Life Sci* 1986;39:1479–1485.
- Petrasek J, Bala S, Csak T, et al. IL-1 receptor antagonist ameliorates inflammasome-dependent alcoholic steatohepatitis in mice. *J Clin Invest* 2012;122:3476–3489.
- Ju C, Mandrekar P. Macrophages and alcohol-related liver inflammation. *Alcohol Res* 2015;37:251–262.
- Kirpich IA, Warner DR, Feng W, et al. Mechanisms, biomarkers and targets for therapy in alcohol-associated liver injury: from genetics to nutrition—summary of the ISBRA 2018 symposium. *Alcohol* 2020;83:105–114.
- Bajaj JS, Hylemon PB. Gut-liver axis alterations in alcoholic liver disease: are bile acids the answer? *Hepatology* 2018;67:2074–2075.
- Szabo G. Gut-liver axis in alcoholic liver disease. *Gastroenterology* 2015;148:30–36.
- Milosevic I, Vujovic A, Barac A, et al. Gut-liver axis, gut microbiota, and its modulation in the management of liver diseases: a review of the literature. *Int J Mol Sci* 2019;20.
- Shao T, Zhao C, Li F, et al. Intestinal HIF-1 $\alpha$  deletion exacerbates alcoholic liver disease by inducing intestinal dysbiosis and barrier dysfunction. *J Hepatol* 2018;69:886–895.
- Rao R. Endotoxemia and gut barrier dysfunction in alcoholic liver disease. *Hepatology* 2009;50:638–644.
- Keshavarzian A, Farhadi A, Forsyth CB, et al. Evidence that chronic alcohol exposure promotes intestinal oxidative stress, intestinal hyperpermeability and endotoxemia prior to development of alcoholic steatohepatitis in rats. *J Hepatol* 2009;50:538–547.
- Andersson U, Tracey KJ. HMGB1 is a therapeutic target for sterile inflammation and infection. *Annu Rev Immunol* 2011;29:139–162.
- Bianchi ME. HMGB1 loves company. *J Leukoc Biol* 2009;86:573–576.
- Sims GP, Rowe DC, Rietdijk ST, et al. HMGB1 and RAGE in inflammation and cancer. *Annu Rev Immunol* 2010;28:367–388.
- Seong SY, Matzinger P. Hydrophobicity: an ancient damage-associated molecular pattern that initiates innate immune responses. *Nature Reviews Immunology* 2004;4:469–478.
- Zeh HJ 3rd, Lotze MT. Addicted to death: invasive cancer and the immune response to unscheduled cell death. *J Immunother* 2005;28:1–9.
- Han H, Desert R, Das S, et al. Danger signals in liver injury and restoration of homeostasis. *J Hepatol* 2020;73:933–951.
- Dumitriu IE, Baruah P, Manfredi AA, et al. HMGB1: guiding immunity from within. *Trends Immunol* 2005;26:381–387.
- Takino J, Nagamine K, Hori T, et al. Contribution of the toxic advanced glycation end-products-receptor axis in nonalcoholic steatohepatitis-related hepatocellular carcinoma. *World J Hepatol* 2015;7:2459–2469.
- Arriazu E, Ge X, Leung TM, et al. Signalling via the osteopontin and high mobility group box-1 axis drives the fibrogenic response to liver injury. *Gut* 2017;66:1123–1137.
- Yamagishi S, Matsui T. Role of receptor for advanced glycation end products (RAGE) in liver disease. *Eur J Med Res* 2015;20:15.
- Sun L, Dai JJ, Hu WF, et al. Expression of toll-like receptors in hepatic cirrhosis and hepatocellular carcinoma. *Genet Mol Res* 2016;15.
- Ito I, Fukazawa J, Yoshida M. Post-translational methylation of high mobility group box 1 (HMGB1) causes its cytoplasmic localization in neutrophils. *J Biol Chem* 2007;282:16336–16344.
- Oh YJ, Youn JH, Ji Y, et al. HMGB1 is phosphorylated by classical protein kinase C and is secreted by a calcium-dependent mechanism. *J Immunol* 2009;182:5800–5809.
- Yang H, Hreggvidsdottir HS, Palmblad K, et al. A critical cysteine is required for HMGB1 binding to Toll-like

- receptor 4 and activation of macrophage cytokine release. *Proc Natl Acad Sci U S A* 2010;107, 11942–11947.
30. Yang H, Lundback P, Ottosson L, et al. Redox modification of cysteine residues regulates the cytokine activity of high mobility group box-1 (HMGB1). *Mol Med* 2012;18:250–259.
  31. Tilg H, Wilmer A, Vogel W, et al. Serum levels of cytokines in chronic liver diseases. *Gastroenterology* 1992; 103:264–274.
  32. Sekiyama KD, Yoshida M, Thomson AW. Circulating proinflammatory cytokines (IL-1 beta, TNF-alpha, and IL-6) and IL-1 receptor antagonist (IL-1Ra) in fulminant hepatic failure and acute hepatitis. *Clin Exp Immunol* 1994; 98:71–77.
  33. Agalave NM, Larsson M, Abdelmoaty S, et al. Spinal HMGB1 induces TLR4-mediated long-lasting hypersensitivity and glial activation and regulates pain-like behavior in experimental arthritis. *Pain* 2014; 155:1802–1813.
  34. Ge X, Arriazu E, Magdaleno F, et al. High mobility group box-1 drives fibrosis progression signaling via the receptor for advanced glycation end products in mice. *Hepatology* 2018;68:2380–2404.
  35. Boetticher NC, Peine CJ, Kwo P, et al. A randomized, double-blinded, placebo-controlled multicenter trial of etanercept in the treatment of alcoholic hepatitis. *Gastroenterology* 2008;135:1953–1960.
  36. Szabo G. Gut-liver axis beyond the microbiome: how the fungal mycobiome contributes to alcoholic liver disease. *Hepatology* 2018;68:2426–2428.
  37. Adolph TE, Grander C, Moschen AR, et al. Liver-microbiome axis in health and disease. *Trends Immunol* 2018; 39:712–723.
  38. Hartmann P, Hochrath K, Horvath A, et al. Modulation of the intestinal bile acid/farnesoid X receptor/fibroblast growth factor 15 axis improves alcoholic liver disease in mice. *Hepatology* 2018;67:2150–2166.
  39. Huang H, Nace GW, McDonald KA, et al. Hepatocyte-specific high-mobility group box 1 deletion worsens the injury in liver ischemia/reperfusion: a role for intracellular high-mobility group box 1 in cellular protection. *Hepatology* 2014;59:1984–1997.
  40. Shao L, Ling Z, Chen D, et al. Disorganized gut microbiome contributed to liver cirrhosis progression: a metagenomics-based study. *Front Microbiol* 2018;9:3166.
  41. Fisher NC, Neil DA, Williams A, et al. Serum concentrations and peripheral secretion of the beta chemokines monocyte chemoattractant protein 1 and macrophage inflammatory protein 1alpha in alcoholic liver disease. *Gut* 1999;45:416–420.
  42. Dominguez M, Miquel R, Colmenero J, et al. Hepatic expression of CXC chemokines predicts portal hypertension and survival in patients with alcoholic hepatitis. *Gastroenterology* 2009;136:1639–1650.
  43. Afford SC, Fisher NC, Neil DA, et al. Distinct patterns of chemokine expression are associated with leukocyte recruitment in alcoholic hepatitis and alcoholic cirrhosis. *J Pathol* 1998;186:82–89.
  44. Mandrekar P, Ambade A, Lim A, et al. An essential role for monocyte chemoattractant protein-1 in alcoholic liver injury: regulation of proinflammatory cytokines and hepatic steatosis in mice. *Hepatology* 2011;54:2185–2197.
  45. Gaskell H, Ge X, Desert R, et al. Ablation of Hmgb1 in intestinal epithelial cells causes intestinal lipid accumulation and reduces NASH in mice. *Hepatol Commun* 2020;4:92–108.
  46. Ge X, Desert R, Magdaleno F, et al. Redox-sensitive high-mobility group box-1 isoforms contribute to liver fibrosis progression and resolution in mice. *J Hepatol* 2024;80:482–494.
  47. Urtasun R, Lopategi A, George J, et al. Osteopontin, an oxidant stress sensitive cytokine, up-regulates collagen-I via integrin alpha(V)beta(3) engagement and PI3K/pAkt/NFkappaB signaling. *Hepatology* 2012;55:594–608.
  48. Wang X, Lopategi A, Ge X, et al. Osteopontin induces ductular reaction contributing to liver fibrosis. *Gut* 2014; 63:1805–1818.
  49. Ge X, Leung TM, Arriazu E, et al. Osteopontin binding to lipopolysaccharide lowers tumor necrosis factor-alpha and prevents early alcohol-induced liver injury in mice. *Hepatology* 2014;59:1600–1616.
  50. Constien R, Forde A, Liliensiek B, et al. Characterization of a novel EGFP reporter mouse to monitor Cre recombination as demonstrated by a Tie2 Cre mouse line. *Genesis* 2001;30:36–44.
  51. Sodhi CP, Neal MD, Siggers R, et al. Intestinal epithelial Toll-like receptor 4 regulates goblet cell development and is required for necrotizing enterocolitis in mice. *Gastroenterology* 2012;143:708–718 e5.
  52. Lieber CS, DeCarli LM. The feeding of alcohol in liquid diets: two decades of applications and 1982 update. *Alcohol Clin Exp Res* 1982;6:523–531.
  53. Chandler RJ, Tarasenko TN, Cusmano-Ozog K, et al. Liver-directed adeno-associated virus serotype 8 gene transfer rescues a lethal murine model of citrullinemia type 1. *Gene Ther* 2013;20:1188–1191.
  54. Yan Z, Yan H, Ou H. Human thyroxine binding globulin (TBG) promoter directs efficient and sustaining transgene expression in liver-specific pattern. *Gene* 2012; 506:289–294.
  55. Erben U, Loddenkemper C, Doerfel K, et al. A guide to histomorphological evaluation of intestinal inflammation in mouse models. *Int J Clin Exp Pathol* 2014;7:4557–4576.
  56. Nieto N. Oxidative-stress and IL-6 mediate the fibrogenic effects of [corrected] Kupffer cells on stellate cells. *Hepatology* 2006;44:1487–1501.
  57. Cubero FJ, Nieto N. Ethanol and arachidonic acid synergize to activate Kupffer cells and modulate the fibrogenic response via tumor necrosis factor alpha, reduced glutathione, and transforming growth factor beta-dependent mechanisms. *Hepatology* 2008;48:2027–2039.
  58. Trapnell C, Roberts A, Goff L, et al. Differential gene and transcript expression analysis of RNA-seq experiments with TopHat and Cufflinks. *Nat Protoc* 2012;7:562–578.

---

Received January 3, 2024. Accepted May 16, 2024.

**Correspondence**

Address correspondence to: Natalia Nieto, PhD, Department of Pathology, University of Illinois Chicago, 840 South Wood Street, Suite 130 CSN, MC 847, Chicago, Illinois 60612. e-mail: nniето@uic.edu.

**Acknowledgments**

The authors thank Dr Timothy R. Billiar (University of Pittsburgh, Pittsburgh, Pennsylvania) for donating the *Hmgb1<sup>fl/fl</sup>* mice, Dr Bernd Arnold (German Cancer Research Center, Heidelberg, Germany) for providing the *Rage<sup>fl/fl</sup>* mice, and Dr David J. Hackam (University of Pittsburgh, Pittsburgh, Pennsylvania) for donating the *Tlr4<sup>fl/fl</sup>* mice. They thank Dr Hyun Lee (Director, UIC Biophysics Core) for her assistance in the Surface Plasmon Resonance studies.

**CRediT Authorship Contributions**

Xiaodong Ge, PhD, MD (Data curation: Lead; Formal analysis: Lead; Methodology: Lead; Project administration: Lead; Software: Equal; Supervision: Equal)

Hui Han, PhD (Methodology: Supporting)

Romain Desert, PhD (Software: Supporting)

Sukanta Das, PhD (Methodology: Supporting)

Zhuolun Song, PhD, MD (Methodology: Supporting)

Sai Santosh Babu Komakula, PhD (Methodology: Supporting)

Wei Chen, PhD (Methodology: Supporting)

Dipti Athavale, PhD (Methodology: Supporting)

Daniel Lantvit, Bachelor (Methodology: Supporting)

Natalia Nieto, PhD (Funding acquisition: Lead; Investigation: Lead; Supervision: Lead; Writing – original draft: Lead)

**Conflicts of interest**

The authors disclose no conflicts.

**Funding**

Supported by US Public Health Service Grant R01AA025907 from the National Institute on Alcohol Abuse and Alcoholism (Natalia Nieto) and US Veterans Administration Grant I01BX005093 from the Biomedical Laboratory Research & Development (Natalia Nieto). The views expressed in this article are those of the authors and do not necessarily reflect the position or policy of the Department of Veterans Affairs or the US government.